Making sense of data: introduction to statistics for gravitational wave astronomy

Lecture 8: Examples of Bayesian statistics in GW data analysis

AEI IMPRS Lecture Course

Jonathan Gair jgair@aei.mpg.de

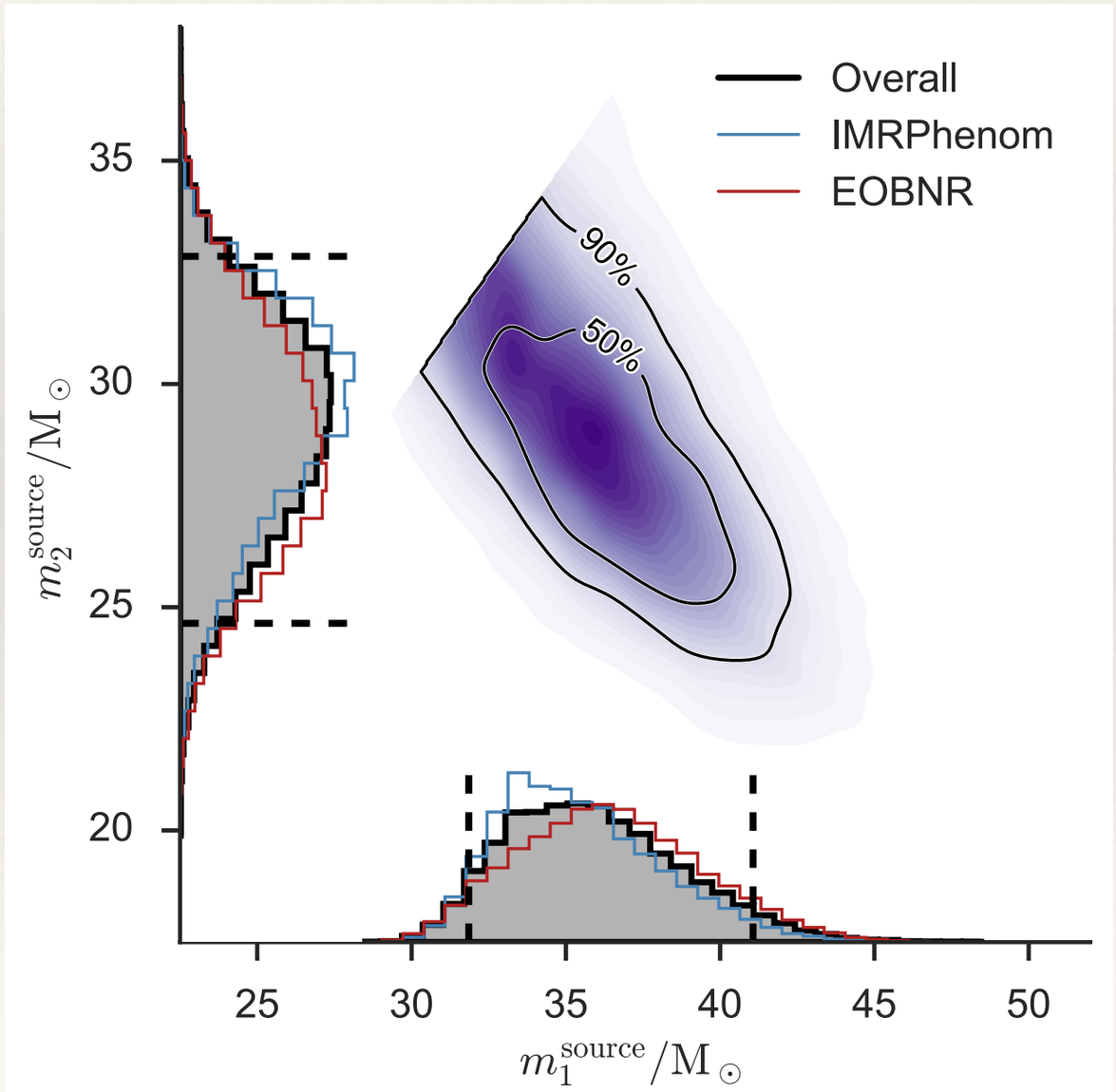

Parameter Estimation: LIGO

LIGO Parameter Estimation

- LIGO parameter estimation uses Bayesian methods. Results are quoted as posterior distributions, or posterior median values and credible intervals.

Event	$m_1/M_\odot$	$m_2/M_\odot$	$\mathcal{M}/M_\odot$	$\chi_{\rm eff}$	$M_f/M_\odot$	a_f	$E_{\rm rad}/(M_\odot c^2)$	$\ell_{\rm peak}/({\rm erg\,s^{-1}})$	$d_L/{\rm Mpc}$	z	$\Delta\Omega/{\rm deg}^2$
GW150914	$35.6^{+4.7}_{-3.1}$	$30.6^{+3.0}_{-4.4}$	$28.6^{+1.7}_{-1.5}$	$-0.01^{+0.12}_{-0.13}$	$63.1^{+3.4}_{-3.0}$	$0.69^{+0.05}_{-0.04}$	$3.1^{+0.4}_{-0.4}$	$3.6^{+0.4}_{-0.4}\times10^{56}$	440^{+150}_{-170}	$0.09^{+0.03}_{-0.03}$	182
GW151012	$23.2^{+14.9}_{-5.5}$	$13.6^{+4.1}_{-4.8}$	$15.2^{+2.1}_{-1.2}$	$0.05^{+0.31}_{-0.20}$	$35.6^{+10.8}_{-3.8}$	$0.67^{+0.13}_{-0.11}$	$1.6^{+0.6}_{-0.5}$	$3.2^{+0.8}_{-1.7}\times10^{56}$	1080^{+550}_{-490}	$0.21^{+0.09}_{-0.09}$	1523
GW151226	$13.7^{+8.8}_{-3.2}$	$7.7^{+2.2}_{-2.5}$	$8.9^{+0.3}_{-0.3}$	$0.18^{+0.20}_{-0.12}$	$20.5^{+6.4}_{-1.5}$	$0.74^{+0.07}_{-0.05}$	$1.0^{+0.1}_{-0.2}$	$3.4^{+0.7}_{-1.7}\times10^{56}$	450^{+180}_{-190}	$0.09^{+0.04}_{-0.04}$	1033
GW170104	$30.8^{+7.3}_{-5.6}$	$20.0^{+4.9}_{-4.6}$	$21.4^{+2.2}_{-1.8}$	$-0.04^{+0.17}_{-0.21}$	$48.9^{+5.1}_{-4.0}$	$0.66^{+0.08}_{-0.11}$	$2.2^{+0.5}_{-0.5}$	$3.3^{+0.6}_{-1.0}\times10^{56}$	990^{+440}_{-430}	$0.20^{+0.08}_{-0.08}$	921
GW170608	$11.0^{+5.5}_{-1.7}$	$7.6^{+1.4}_{-2.2}$	$7.9^{+0.2}_{-0.2}$	$0.03^{+0.19}_{-0.07}$	$17.8^{+3.4}_{-0.7}$	$0.69^{+0.04}_{-0.04}$	$0.9^{+0.0}_{-0.1}$	$3.5^{+0.4}_{-1.3}\times10^{56}$	320^{+120}_{-110}	$0.07^{+0.02}_{-0.02}$	392
GW170729	$50.2^{+16.2}_{-10.2}$	$34.0^{+9.1}_{-10.1}$	$35.4^{+6.5}_{-4.8}$	$0.37^{+0.21}_{-0.25}$	$79.5^{+14.7}_{-10.2}$	$0.81^{+0.07}_{-0.13}$	$4.8^{+1.7}_{-1.7}$	$4.2^{+0.9}_{-1.5}\times10^{56}$	2840^{+1400}_{-1360}	$0.49^{+0.19}_{-0.21}$	1041
GW170809	$35.0^{+8.3}_{-5.9}$	$23.8^{+5.1}_{-5.2}$	$24.9^{+2.1}_{-1.7}$	$0.08^{+0.17}_{-0.17}$	$56.3^{+5.2}_{-3.8}$	$0.70^{+0.08}_{-0.09}$	$2.7^{+0.6}_{-0.6}$	$3.5^{+0.6}_{-0.9}\times10^{56}$	1030^{+320}_{-390}	$0.20^{+0.05}_{-0.07}$	308
GW170814	$30.6^{+5.6}_{-3.0}$	$25.2^{+2.8}_{-4.0}$	$24.1^{+1.4}_{-1.1}$	$0.07^{+0.12}_{-0.12}$	$53.2^{+3.2}_{-2.4}$	$0.72^{+0.07}_{-0.05}$	$2.7^{+0.4}_{-0.3}$	$3.7^{+0.4}_{-0.5}\times10^{56}$	600^{+150}_{-220}	$0.12^{+0.03}_{-0.04}$	87
GW170817	$1.46^{+0.12}_{-0.10}$	$1.27^{+0.09}_{-0.09}$	$1.186^{+0.001}_{-0.001}$	$0.00^{+0.02}_{-0.01}$	≤ 2.8	≤ 0.89	≥ 0.04	$\geq 0.1\times10^{56}$	40^{+7}_{-15}	$0.01^{+0.00}_{-0.00}$	16
GW170818	$35.4^{+7.5}_{-4.7}$	$26.7^{+4.3}_{-5.2}$	$26.5^{+2.1}_{-1.7}$	$-0.09^{+0.18}_{-0.21}$	$59.4^{+4.9}_{-3.8}$	$0.67^{+0.07}_{-0.08}$	$2.7^{+0.5}_{-0.5}$	$3.4^{+0.5}_{-0.7}\times10^{56}$	1060^{+420}_{-380}	$0.21^{+0.07}_{-0.07}$	39
GW170823	$39.5^{+11.2}_{-6.7}$	$29.0^{+6.7}_{-7.8}$	$29.2^{+4.6}_{-3.6}$	$0.09^{+0.22}_{-0.26}$	$65.4^{+10.1}_{-7.4}$	$0.72^{+0.09}_{-0.12}$	$3.3^{+1.0}_{-0.9}$	$3.6^{+0.7}_{-1.1}\times10^{56}$	1940^{+970}_{-900}	$0.35^{+0.15}_{-0.15}$	1666

LVC GWTC-1 (2019)

LIGO PE codes

- In O1 and O2, LIGO parameter estimation used the *LALInference* code. This includes two separate algorithms
  - *LALInferenceMCMC*: A Markov Chain Monte Carlo code based on the Metropolis-Hastings algorithm. Proposal distributions are tuned to features of the likelihood expected for CBC inspirals.
  - *LALInferenceNest*: A bespoke nested sampling algorithm. New live points are drawn by evolving mini-MCMC chains until an independent point is obtained.
- During O3 a new software package, *Bilby*, has become available (also with a parallel implementation, *parallel bilby*). The sampling algorithms in *Bilby* are not bespoke. Instead it uses freely available packages such as *dynesty*. LALInference will continue to be used for O3, with *Bilby* used for cross-checks. It is anticipated that Bilby

LIGO PE results: examples

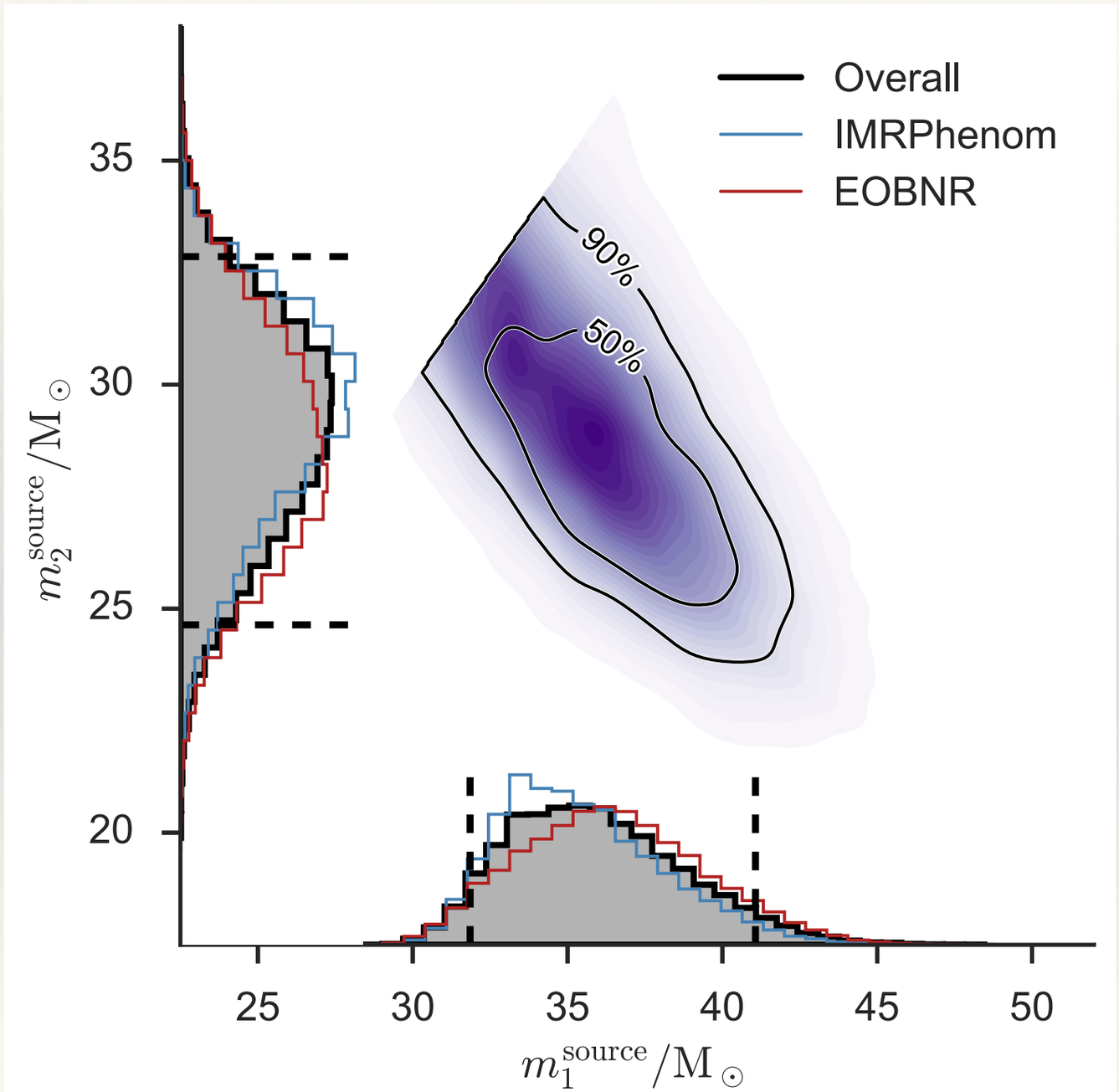

LVC, *Phys. Rev. Lett.* **116**, 061102 (2016)

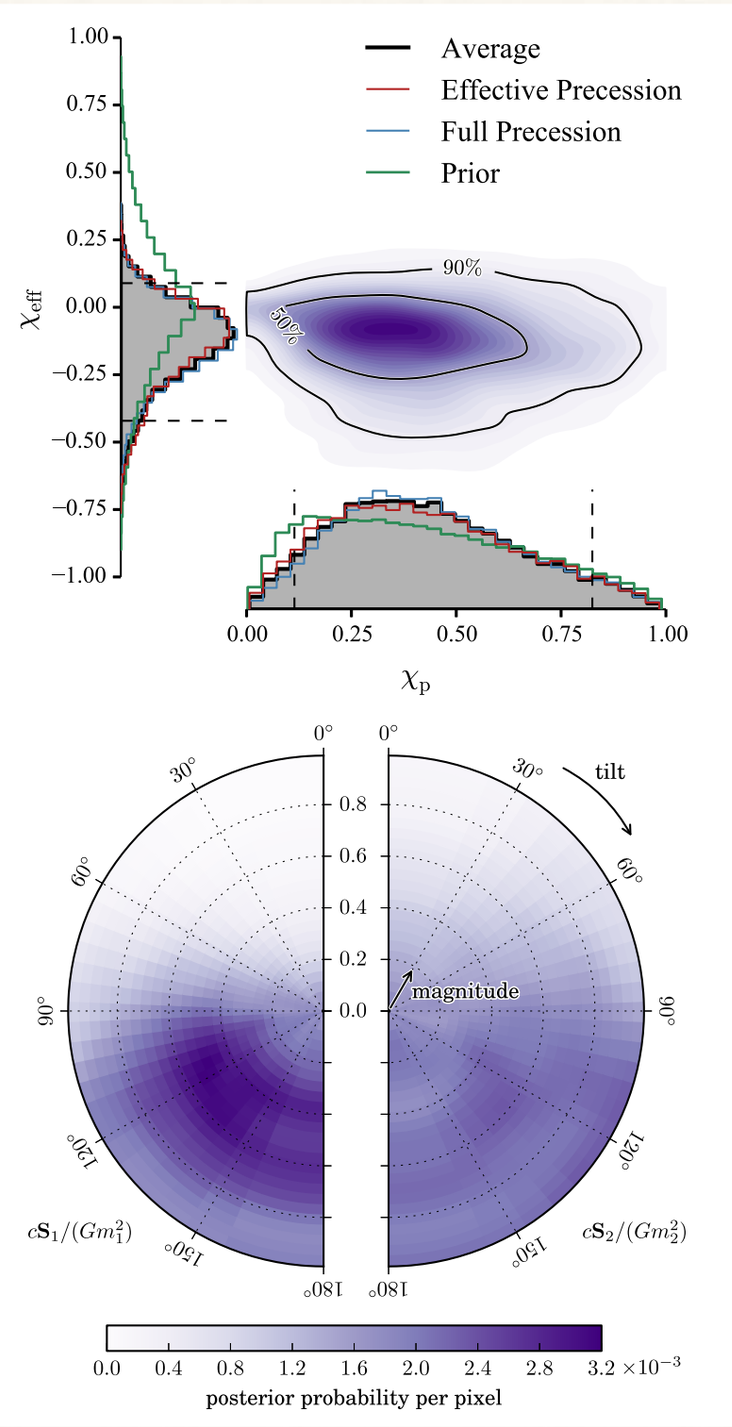

LIGO PE results: examples

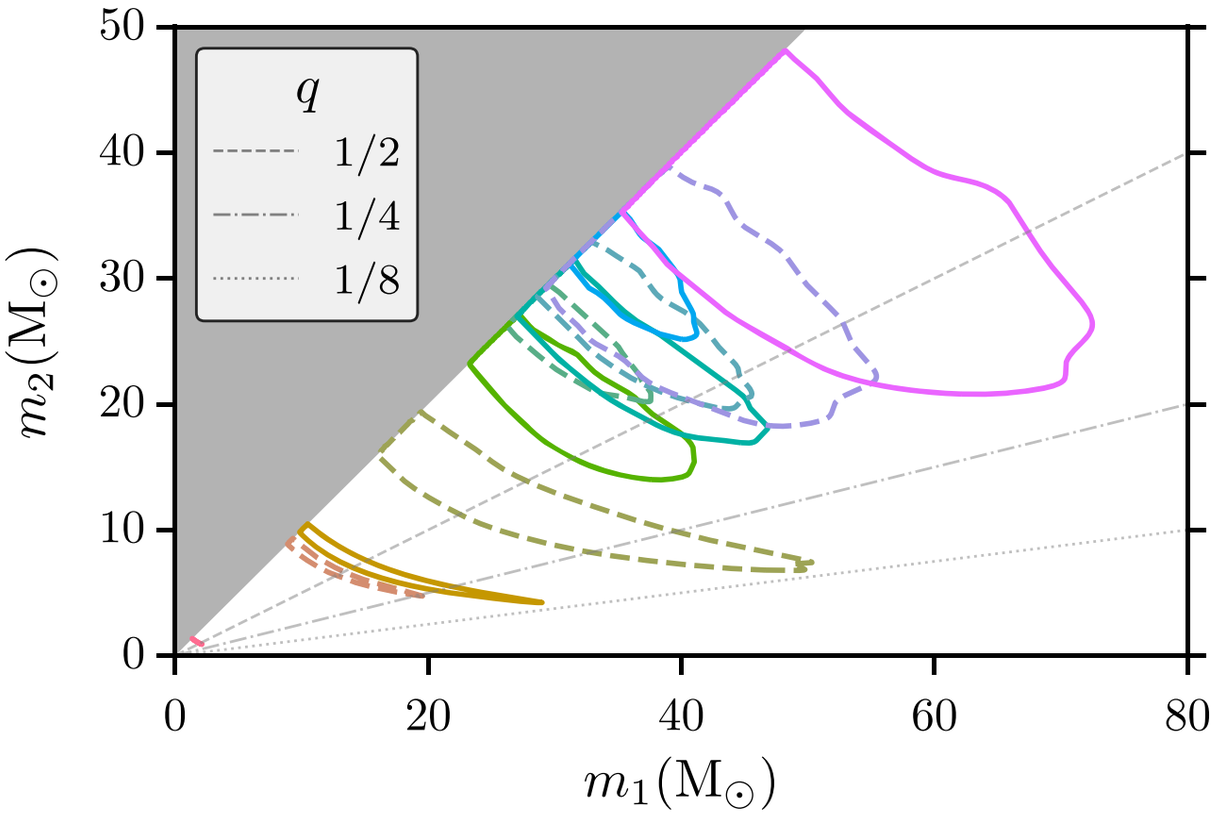

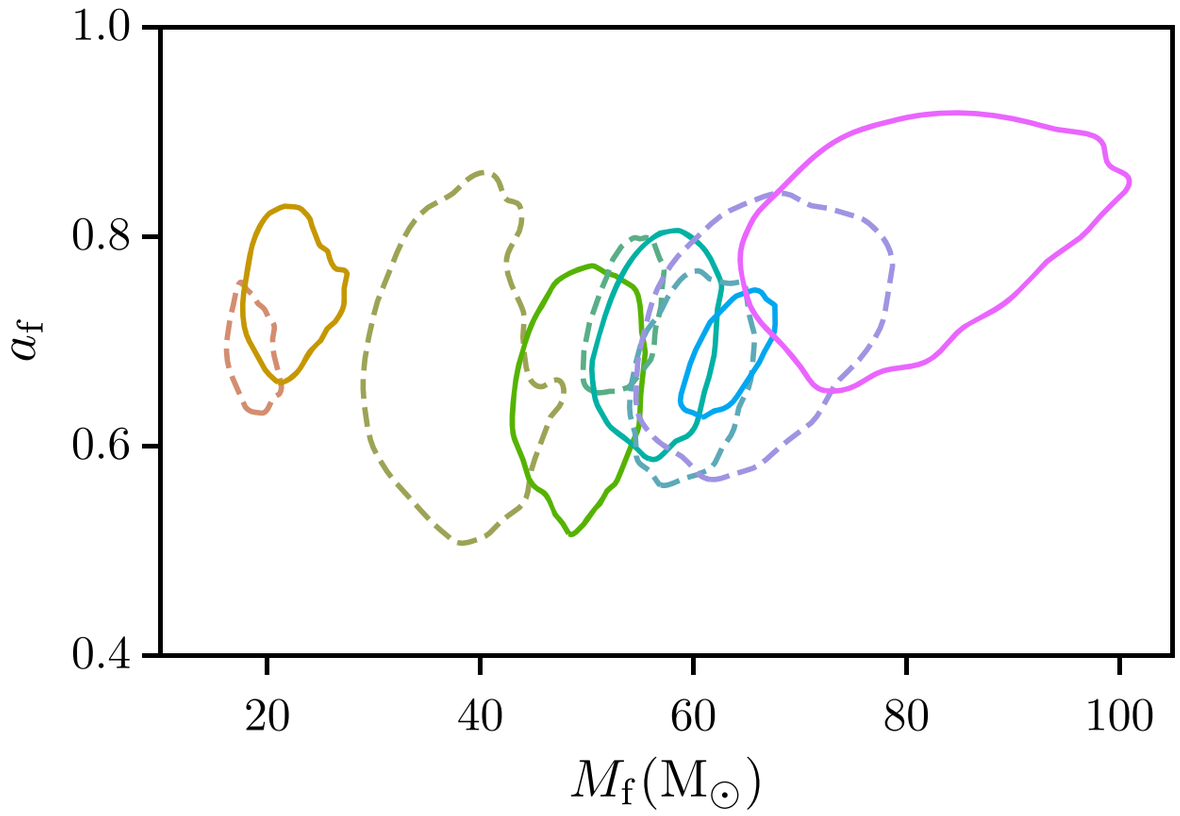

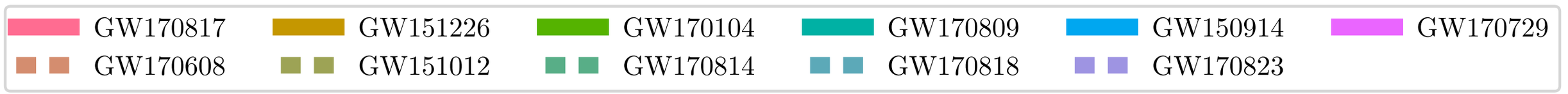

LVC GWTC-1 (2019)

LIGO PE results: examples

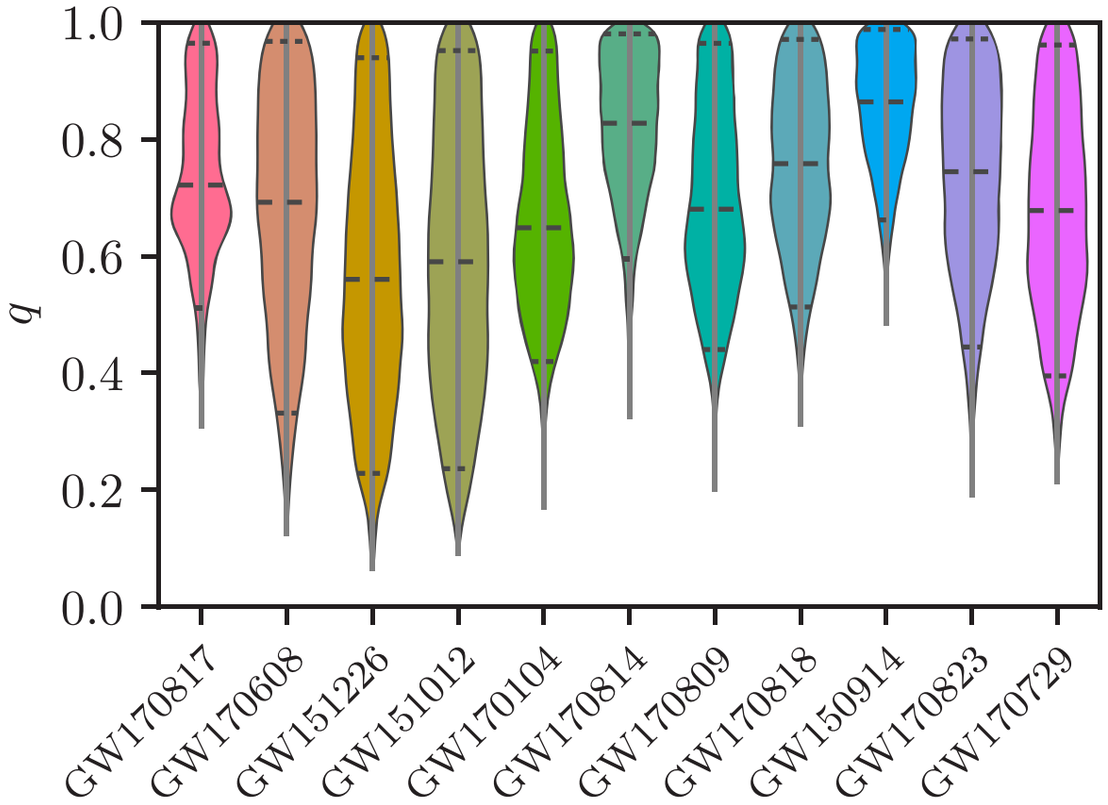

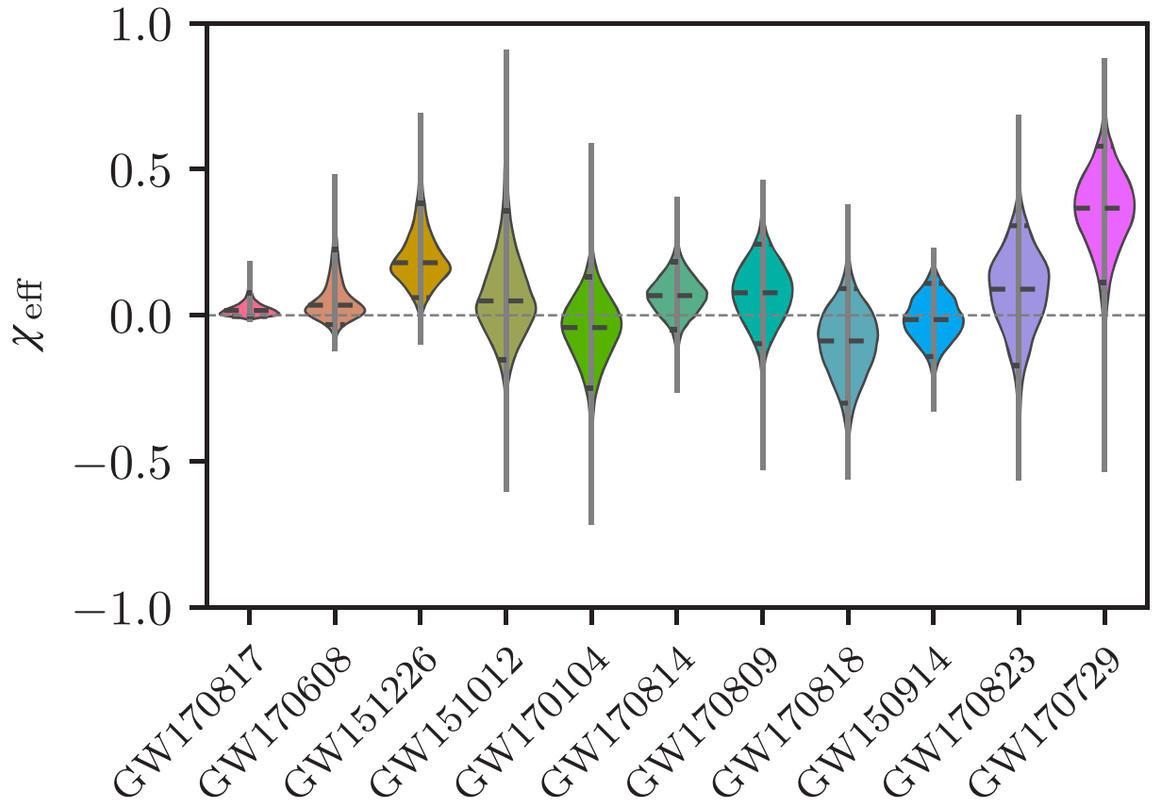

LVC GWTC-1 (2019)

LIGO PE results: examples

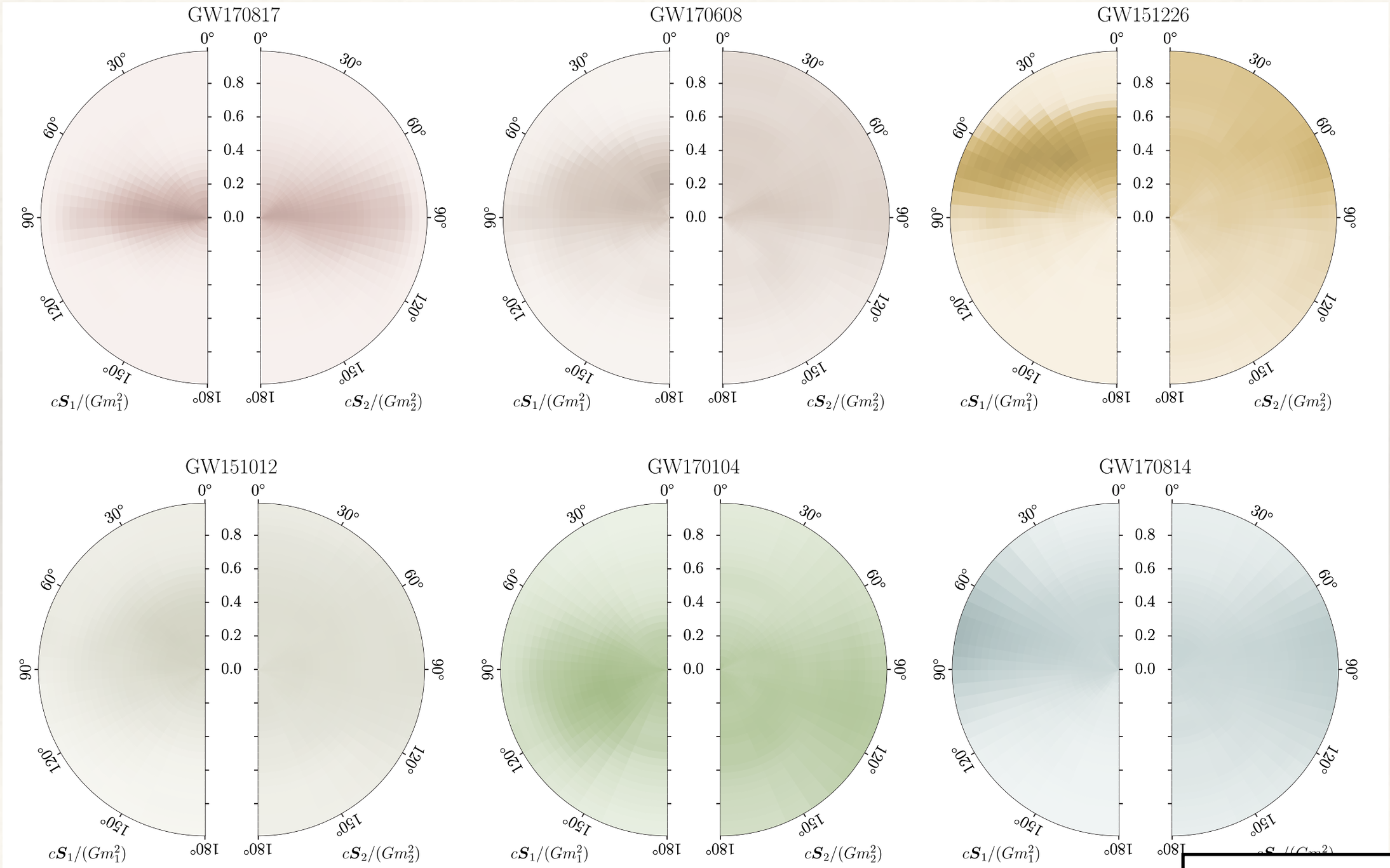

LVC GWTC-1 (2019)

LIGO PE results: examples

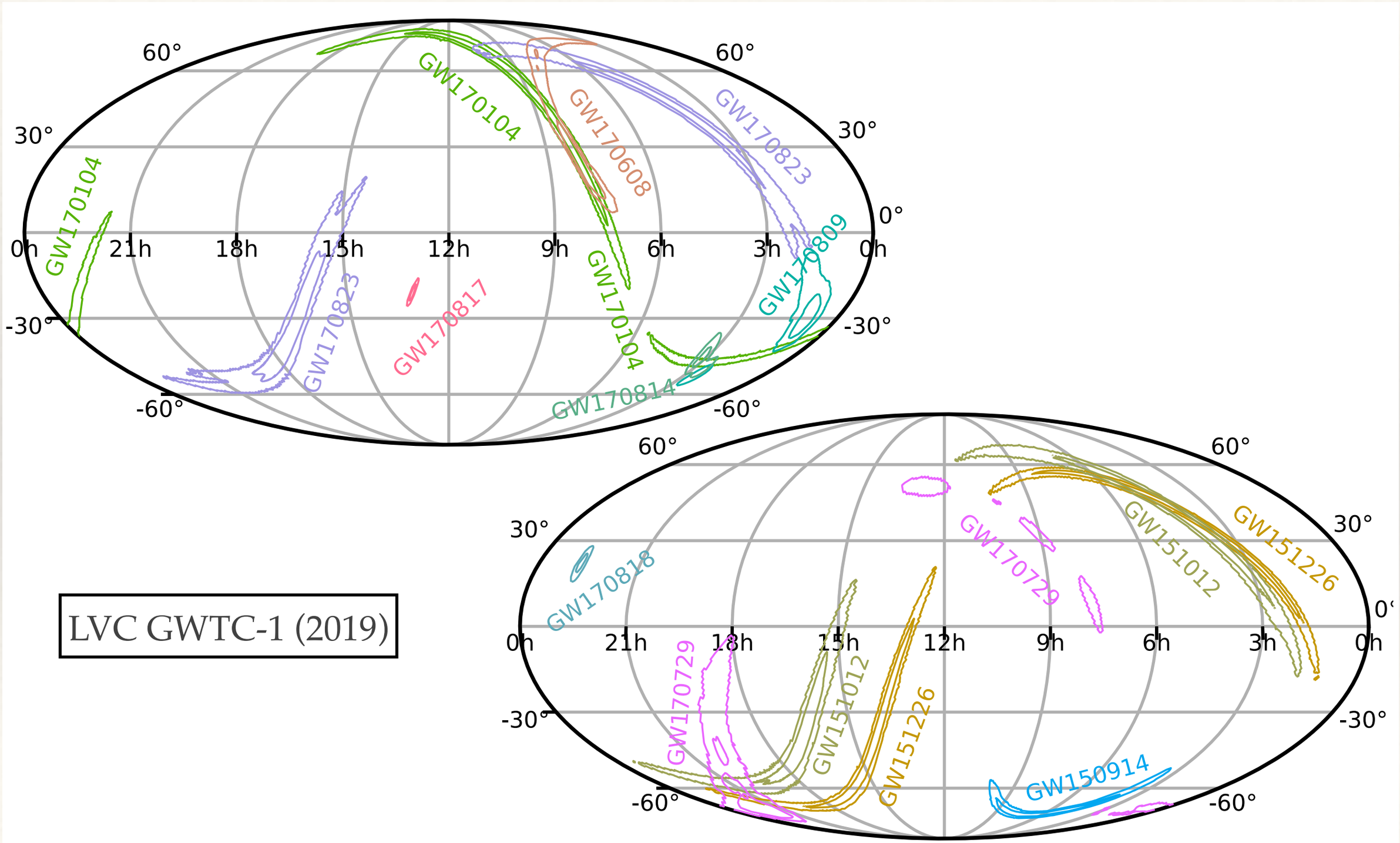

LVC GWTC-1 (2019)

LIGO PE results: examples

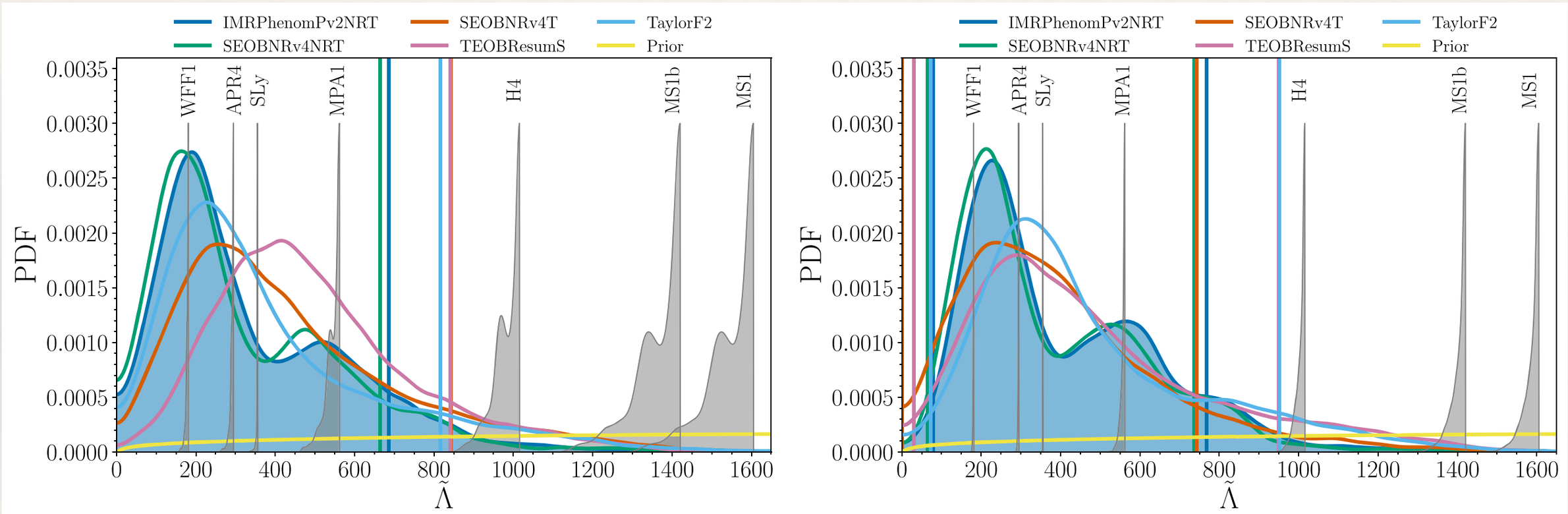

LVC GWTC-1 (2019)

LIGO PE results: examples

- Bayesian methods are also used for tests of general relativity, e.g., to place bounds on pPN deviations in the observed waveform.

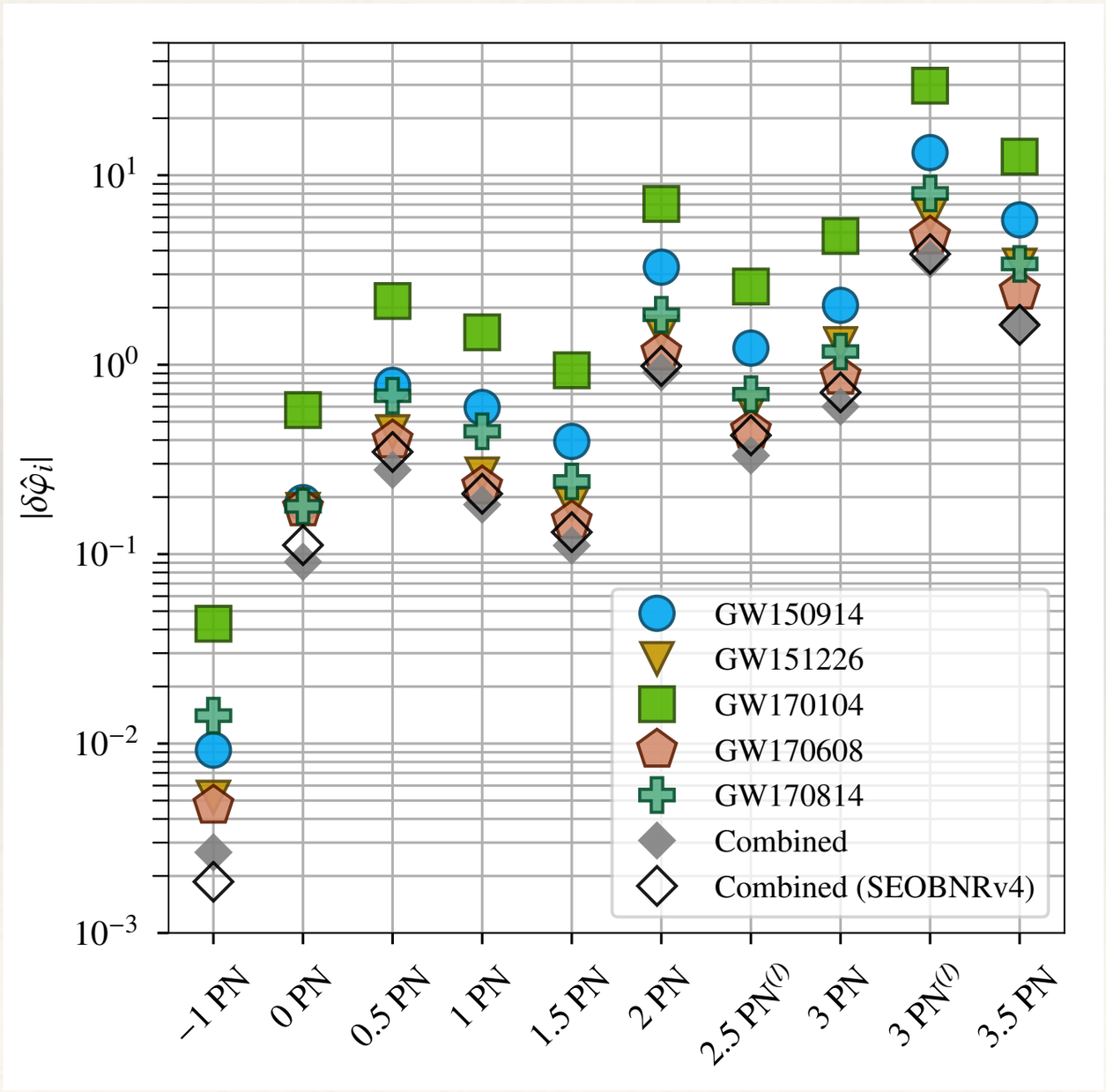

LVC *TGR with GWTC-1* (2019)

Accelerating Inference: Reduced Order Modelling

- Stochastic sampling requires a large number of likelihood evaluations. This can become prohibitively expensive for complex likelihoods or large parameter spaces.
- In a gravitational wave context, **reduced order modelling** has been used to generate develop computationally more efficient likelihood calculations.
- Methods combine a compact representation of the waveform space with an efficient interpolation across parameters (Field, Galley, Pürrer, Tiglio…).
- Typically get order(s) of magnitude computational saving.

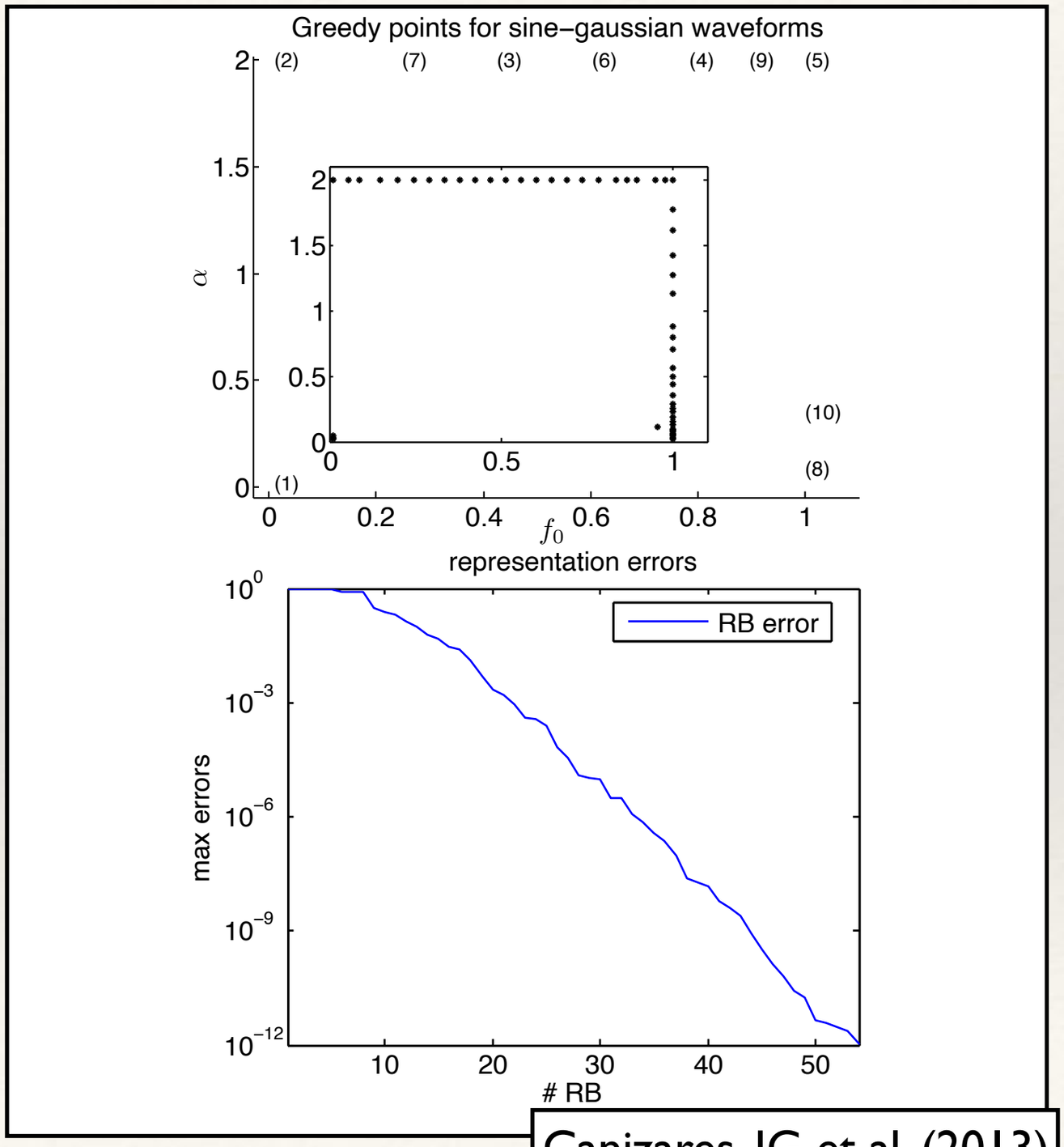

Canizares, JG et al. (2013)

Reduced Order Modelling

- Final step - construct a quadrature rule to approximate overlap

$$(h(\vec{\lambda})|d) = 4\Re \int_0^\infty \frac{\tilde{h}(\vec{\lambda})\tilde{d}^*(f)}{S_h(f)} \mathrm{d}f$$

$$\approx 4\Re \left[\sum_{k=0}^{N/2} d^*(f_k) \vec{e}^T(f_k) \Delta f A^{-1} \right] \vec{h}(\vec{\lambda})$$

$$= 4\Re \sum_{k=1}^{m} \omega_k h(F_k; \vec{\lambda})$$

- **Reduced order quadrature** (ROQ) is state of the art for LIGO PE, but don't have ROQs for all models.

- Models not yet good enough for LISA!

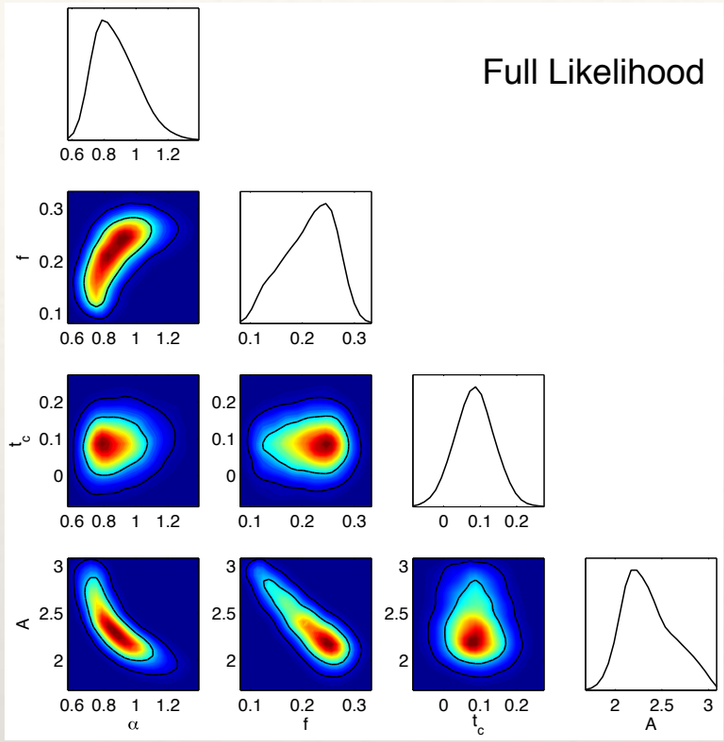

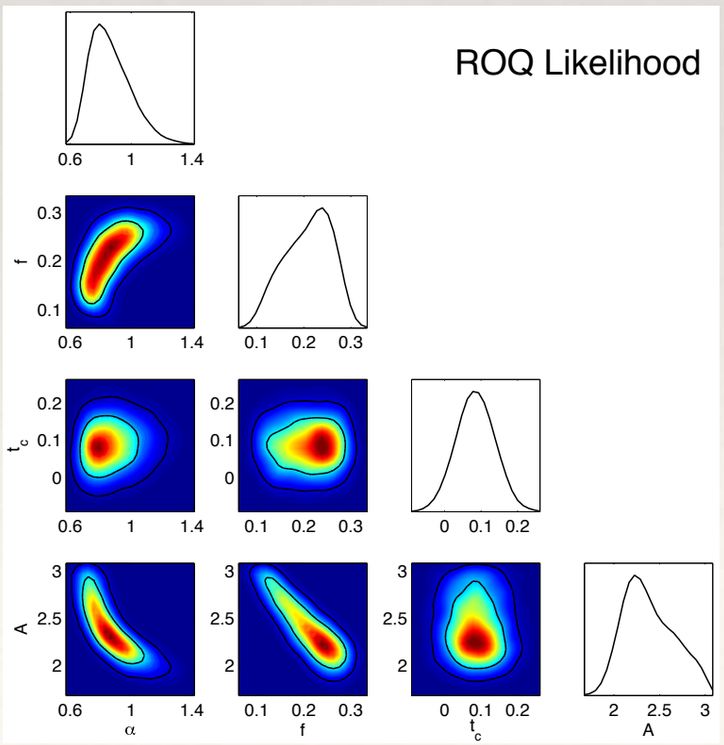

Population Inference

Population Inference

- LIGO employs Bayesian hierarchical models to constrain the parameters of the astrophysical population from which the sources are drawn.
- Examples
  - **Cosmological parameter inference**: estimation of the Hubble constant or other cosmological parameters from sets of events (see lecture 6).
  - **Rate estimation**: estimation of the rate of mergers of different types occurring in the Universe, and its evolution with redshift.
  - **Source population properties**: inference on the distribution of masses and spins of black holes etc.

Rate Estimation

- Alternative approach to rate estimation - simultaneously model foreground and background distributions and try to measure rates.

- Data is a set of observed statistic values, x_i, e.g., max template SNR, evidence etc. Each event has an (unknown) flag, f_i, labelling it as either foreground (f_i =1) or background (f_i =0).

$$d = \{x_i | i = 1, \ldots, N\}$$

- Foreground and background events are Poisson distributed with rates

$$\frac{\mathrm{d}N_f}{\mathrm{d}x} = R_f \hat{f}(x, \theta_f) \qquad \frac{\mathrm{d}N_b}{\mathrm{d}x} = R_b \hat{b}(x, \theta_b)$$

- and corresponding cumulative distributions $\hat{F}(x, \theta_f),\ \hat{B}(x, \theta_b)\,.$

Rate Estimation

- The posterior distribution on flag and rate parameters is

$$p(f_i, R_f, R_b, \theta | d_{\rm to}, N) = \frac{\alpha}{p(d_{\rm to}, N) N!} \left[\prod_{i|f_i=1} R_f \hat{f}(x_i, \theta) \right] \left[\prod_{i|f_i=0} R_b \hat{b}(x_i, \theta) \right] \times \exp[-(R_f + R_b)] \frac{p(\theta)}{\sqrt{R_f R_b}}$$

- For example, consider events ranked by maximum SNR over a template bank with Gaussian noise, with threshold SNR x_{min}.

$$\hat{B}(x) = \frac{\left(1 + \mathrm{erf}\left(\frac{x}{\sqrt{2}}\right)\right)^N - \left(1 + \mathrm{erf}\left(\frac{x_{\rm min}}{\sqrt{2}}\right)\right)^N}{2^N - \left(1 + \mathrm{erf}\left(\frac{x_{\rm min}}{\sqrt{2}}\right)\right)^N} \qquad \hat{F}(x) = 1 - \frac{x_{\rm min}^3}{x^3}$$

- Do not need to identify fore/background events to estimate rates.

Rate Estimation

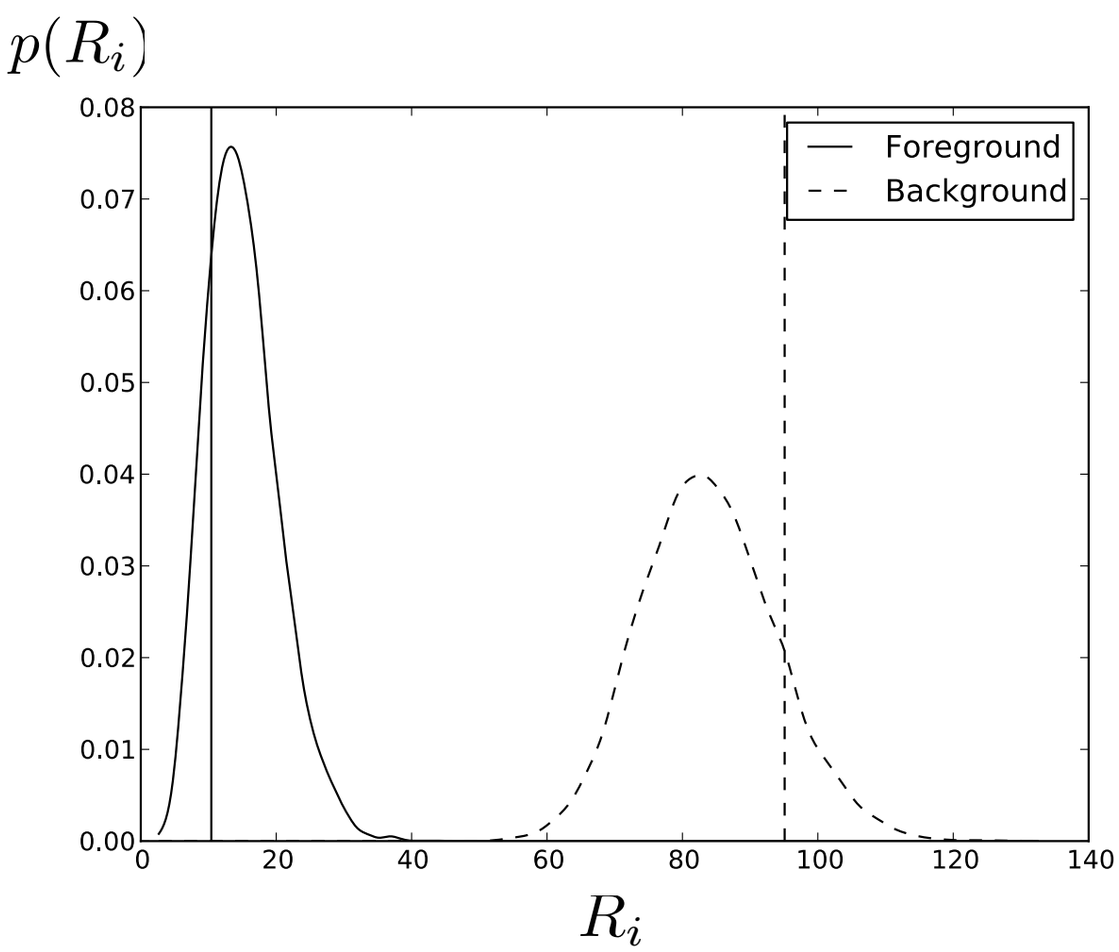

$p(f_i = 1)$

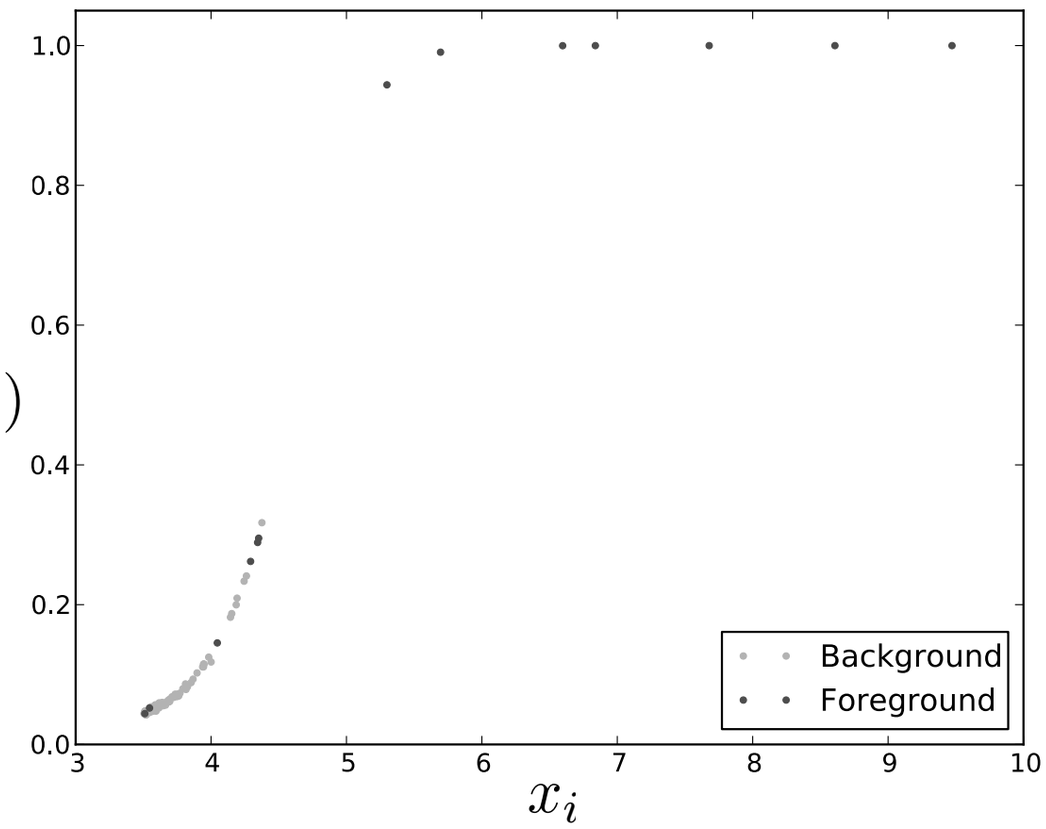

Farr, JG et al. (2014)

Rate Estimation

- The posterior distribution on flag and rate parameters is

$$p(f_i, R_f, R_b, \theta | d_{\rm to}, N) = \frac{\alpha}{p(d_{\rm to}, N) N!} \left[\prod_{i|f_i=1} R_f \hat{f}(x_i, \theta) \right] \left[\prod_{i|f_i=0} R_b \hat{b}(x_i, \theta) \right] \times \exp[-(R_f + R_b)] \frac{p(\theta)}{\sqrt{R_f R_b}}$$

- For example, consider events ranked by maximum SNR over a template bank with Gaussian noise, with threshold SNR x_{min}.

$$\hat{B}(x) = \frac{\left(1 + \mathrm{erf}\left(\frac{x}{\sqrt{2}}\right)\right)^N - \left(1 + \mathrm{erf}\left(\frac{x_{\rm min}}{\sqrt{2}}\right)\right)^N}{2^N - \left(1 + \mathrm{erf}\left(\frac{x_{\rm min}}{\sqrt{2}}\right)\right)^N} \qquad \hat{F}(x) = 1 - \frac{x_{\rm min}^3}{x^3}$$

- Do not need to identify fore/background events to estimate rates.

- Uncertainty in foreground rate is insensitive to threshold.

Rate Estimation

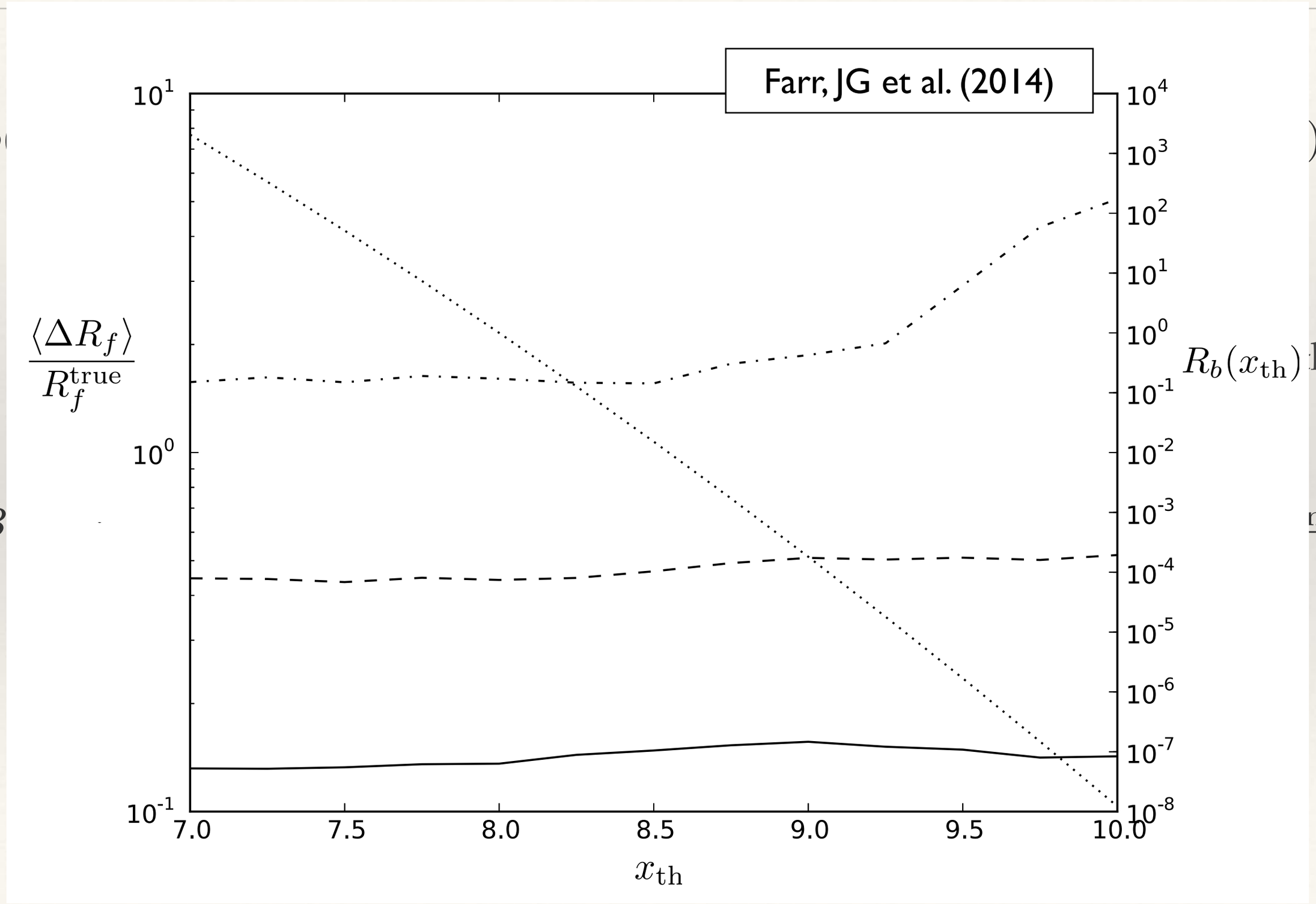

Rate Estimation

- The posterior distribution on flag and rate parameters is

$$p(f_i, R_f, R_b, \theta | d_{\rm to}, N) = \frac{\alpha}{p(d_{\rm to}, N) N!} \left[\prod_{i|f_i=1} R_f \hat{f}(x_i, \theta) \right] \left[\prod_{i|f_i=0} R_b \hat{b}(x_i, \theta) \right] \times \exp[-(R_f + R_b)] \frac{p(\theta)}{\sqrt{R_f R_b}}$$

- For example, consider events ranked by maximum SNR over a template bank with Gaussian noise, with threshold SNR x_{min}.

$$\hat{B}(x) = \frac{\left(1 + \mathrm{erf}\left(\frac{x}{\sqrt{2}}\right)\right)^N - \left(1 + \mathrm{erf}\left(\frac{x_{\rm min}}{\sqrt{2}}\right)\right)^N}{2^N - \left(1 + \mathrm{erf}\left(\frac{x_{\rm min}}{\sqrt{2}}\right)\right)^N} \qquad \hat{F}(x) = 1 - \frac{x_{\rm min}^3}{x^3}$$

- Do not need to identify fore/background events to estimate rates.
- Uncertainty in foreground rate is insensitive to threshold.
- Fore and background can only be separated if they have different shapes. Must assume form or estimate (injections and time-slides?).

Rate estimation: GW150914

- Rate estimation requires foreground distribution. This was complicated for GW150914 by the presence of another, lower significance event, LVT151012.

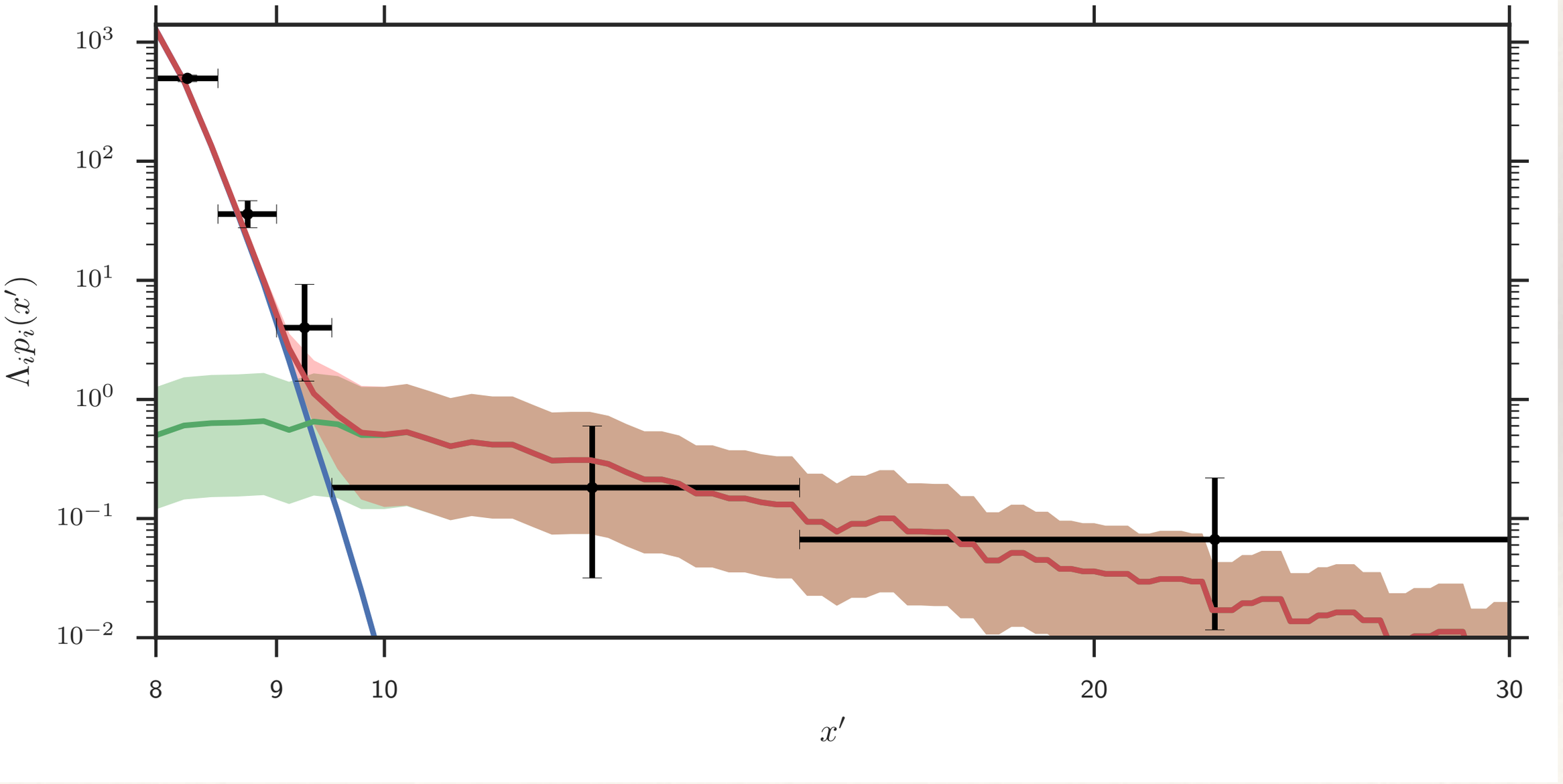

Rate estimation: GW150914

- Parameter estimation follow-up done for the second event (LVT151012) indicates another BBH system, with somewhat lower component masses. This events dominates "alphabet soup" rate estimates.

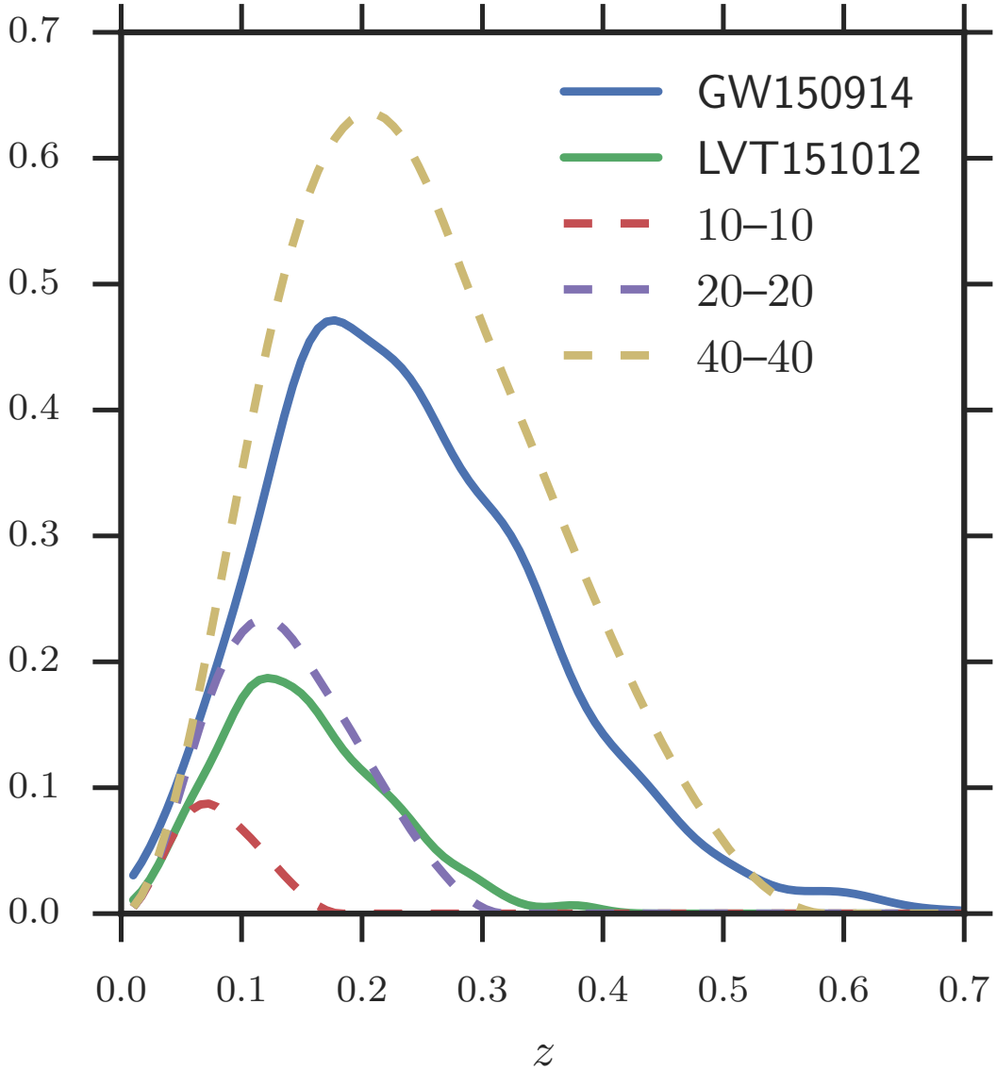

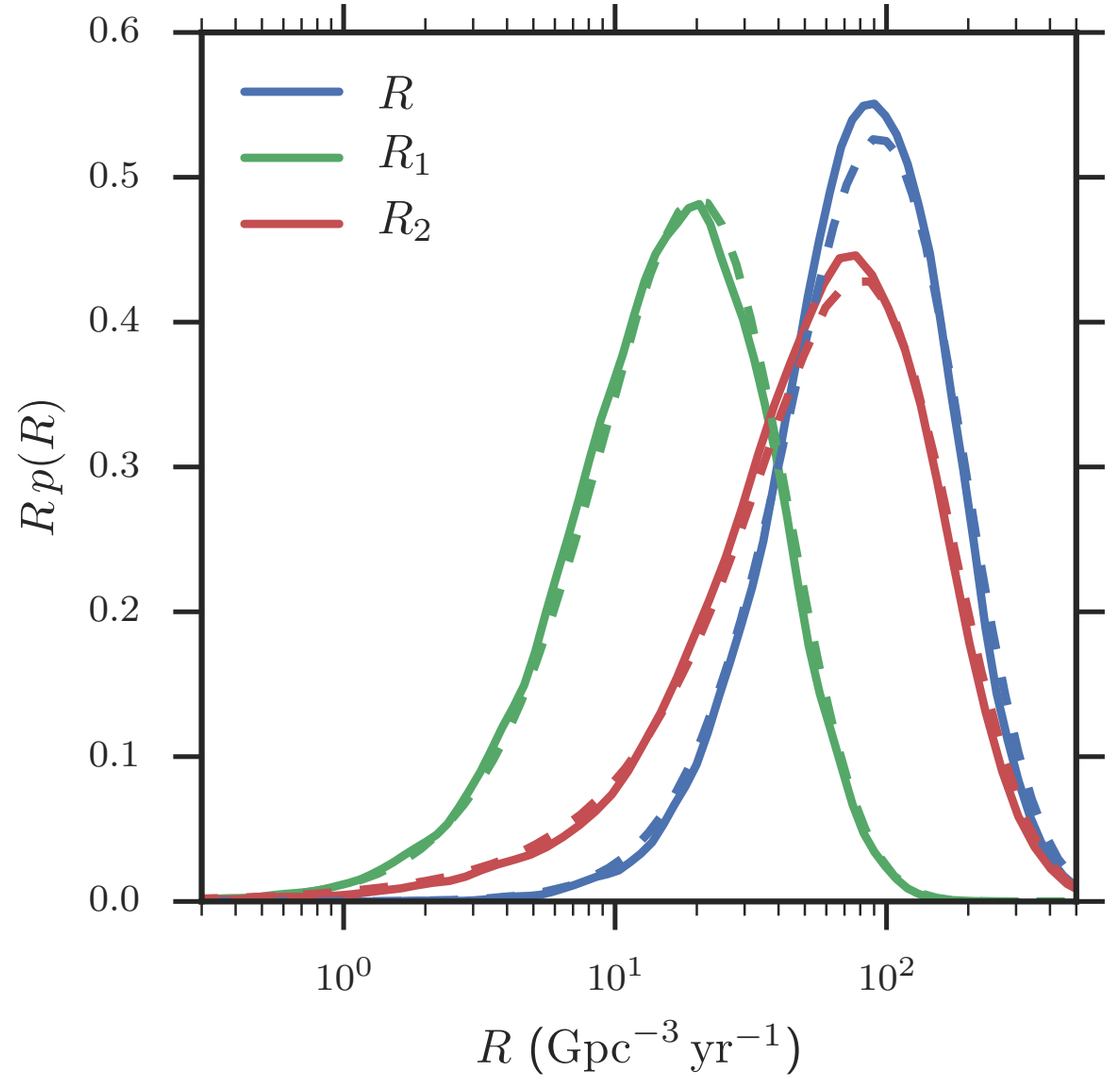

Rate estimation: GW150914

- Estimate rate using three different extrapolations to other BBH systems
- **Reference ("alphabet soup"):** assume all BBHs look like either GW150914 or like LVT151012.
- **Flat:** assume black hole mass distribution is flat in log-mass for both components and uniform in spin.
- **Power-law:** assume $p(m_1) \sim m_1^{-2.35}$ and $q=m_2/m_1$ distributed uniformly.

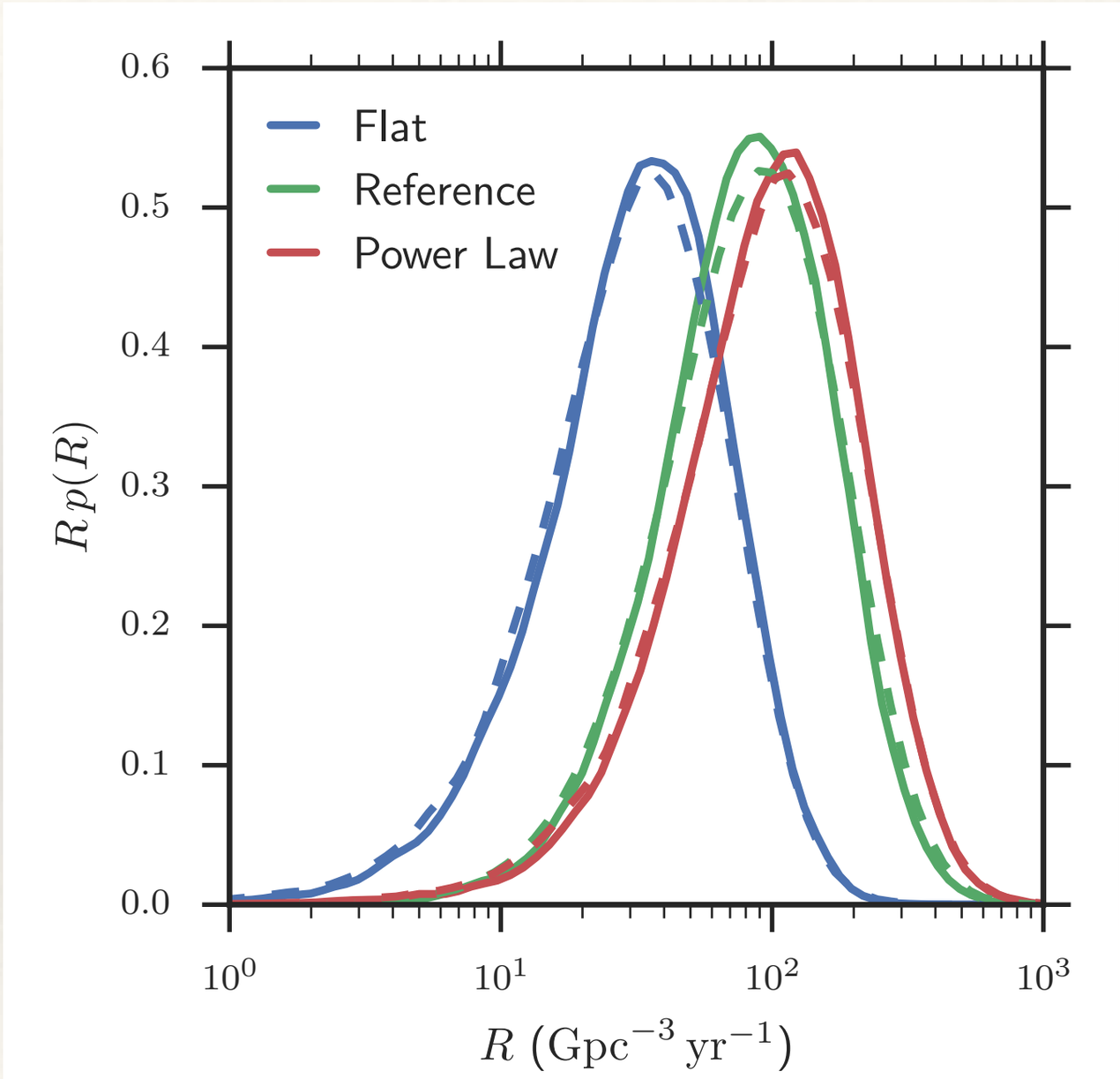

Rate estimation: GW150914

- Final rate estimates.

Mass Distribution	$R/\left(\mathrm{Gpc}^{-3}\,\mathrm{yr}^{-1}\right)$		
	`pycbc`	`gstlal`	Combined
GW150914	16^{+38}_{-13}	17^{+39}_{-14}	17^{+39}_{-13}
LVT151012	61^{+152}_{-53}	62^{+164}_{-55}	62^{+165}_{-54}
Both	82^{+155}_{-61}	84^{+172}_{-64}	83^{+168}_{-63}
Astrophysical			
Flat	33^{+64}_{-26}	32^{+65}_{-25}	33^{+62}_{-26}
Power Law	102^{+198}_{-79}	99^{+203}_{-79}	100^{+201}_{-79}

Rate estimation: GWTC-1

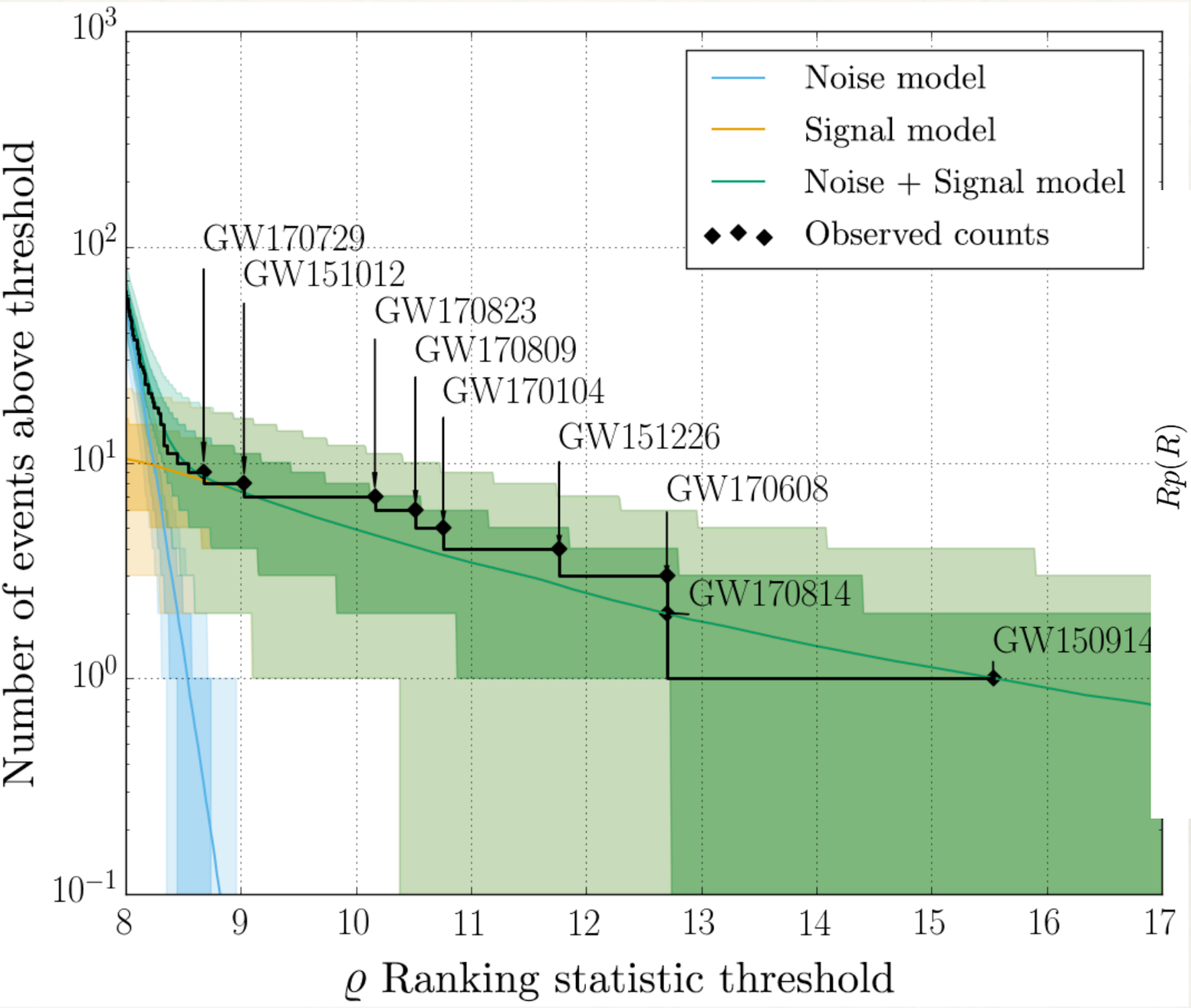

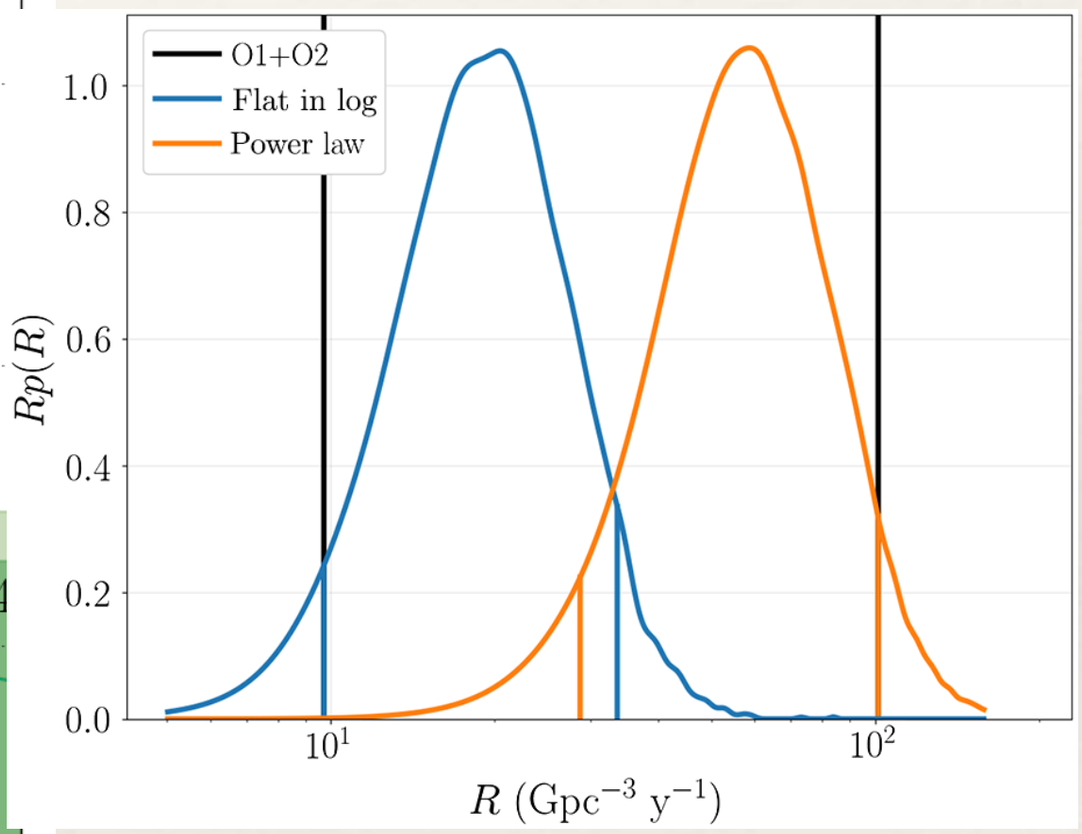

Population inference: masses

- Infer mass distribution of black holes by using hierarchical models with different forms for the mass prior.
- Simplest model is a power law

$$p(m_1, m_2|m_{\rm min}, m_{\rm max}, \alpha, \beta_q) \propto \begin{cases} C(m_1) m_1^{-\alpha} q^{\beta_q} & \text{if } m_{\rm min} \leq m_2 \leq m_1 \leq m_{\rm max} \\ 0 & \text{otherwise} \end{cases}$$

- LIGO analysis uses two variants
  - A: minimum mass fixed to 5 solar masses, flat in mass ratio;
  - B: all parameters allowed to vary.
- Also consider a more sophisticated model designed to identify an excess of black holes at the edge of the pair-instability supernova mass gap

$$p(m_1|\theta) = \left[(1-\lambda_m) A(\theta) m_1^{-\alpha} \Theta(m_{\rm max} - m_1) + \lambda_m B(\theta) \exp\left(-\frac{(m_1-\mu_m)^2}{2\sigma_m^2}\right)\right] S(m_1, m_{\rm min}, \delta m)$$

$$p(q|m_1, \theta) = C(m_1, \theta) q^{\beta_q} S(m_2, m_{\rm min}, \delta m).$$

Population inference: masses

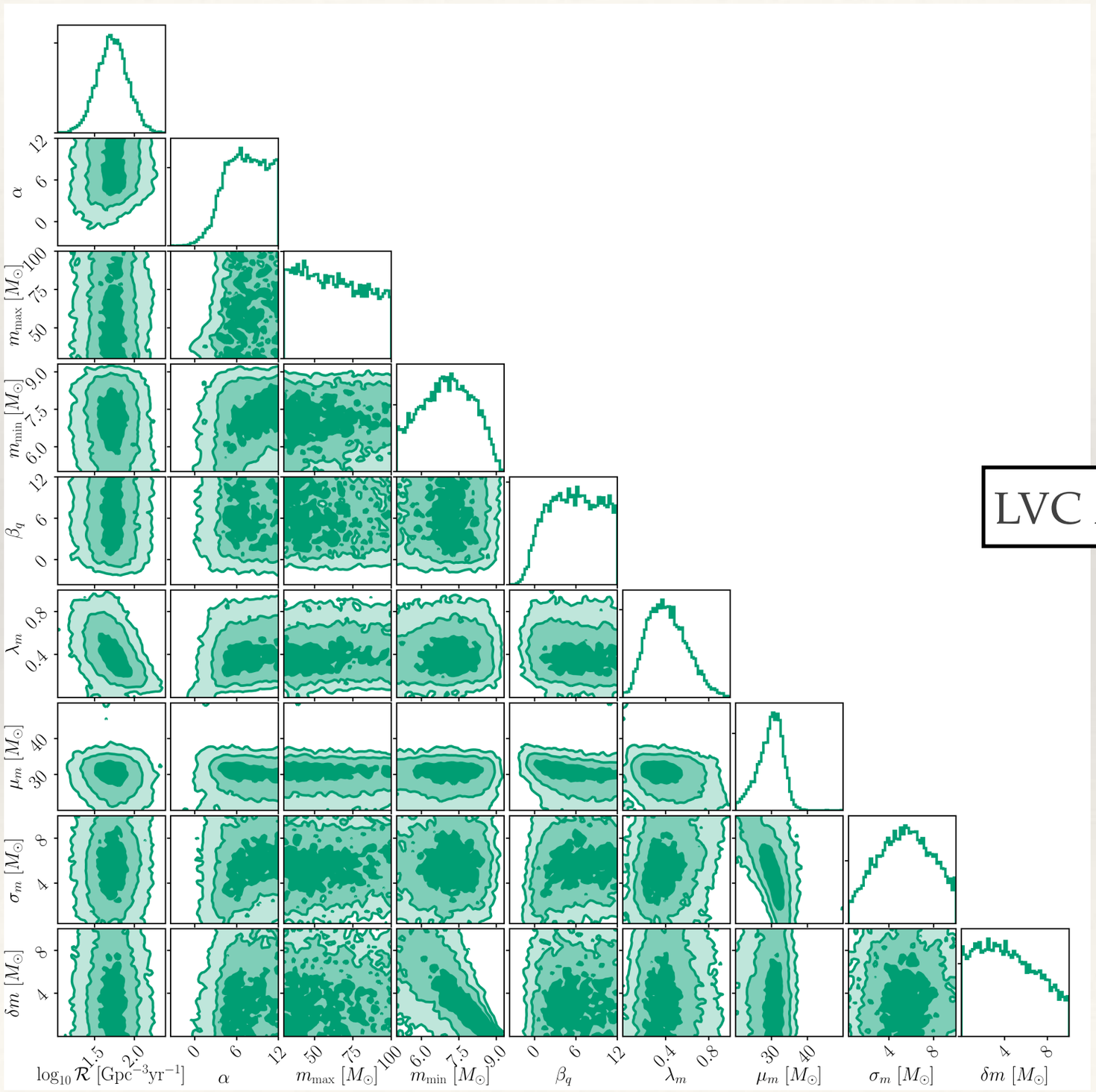

LVC *BBH properties from GWTC-1* (2019)

Population inference: masses

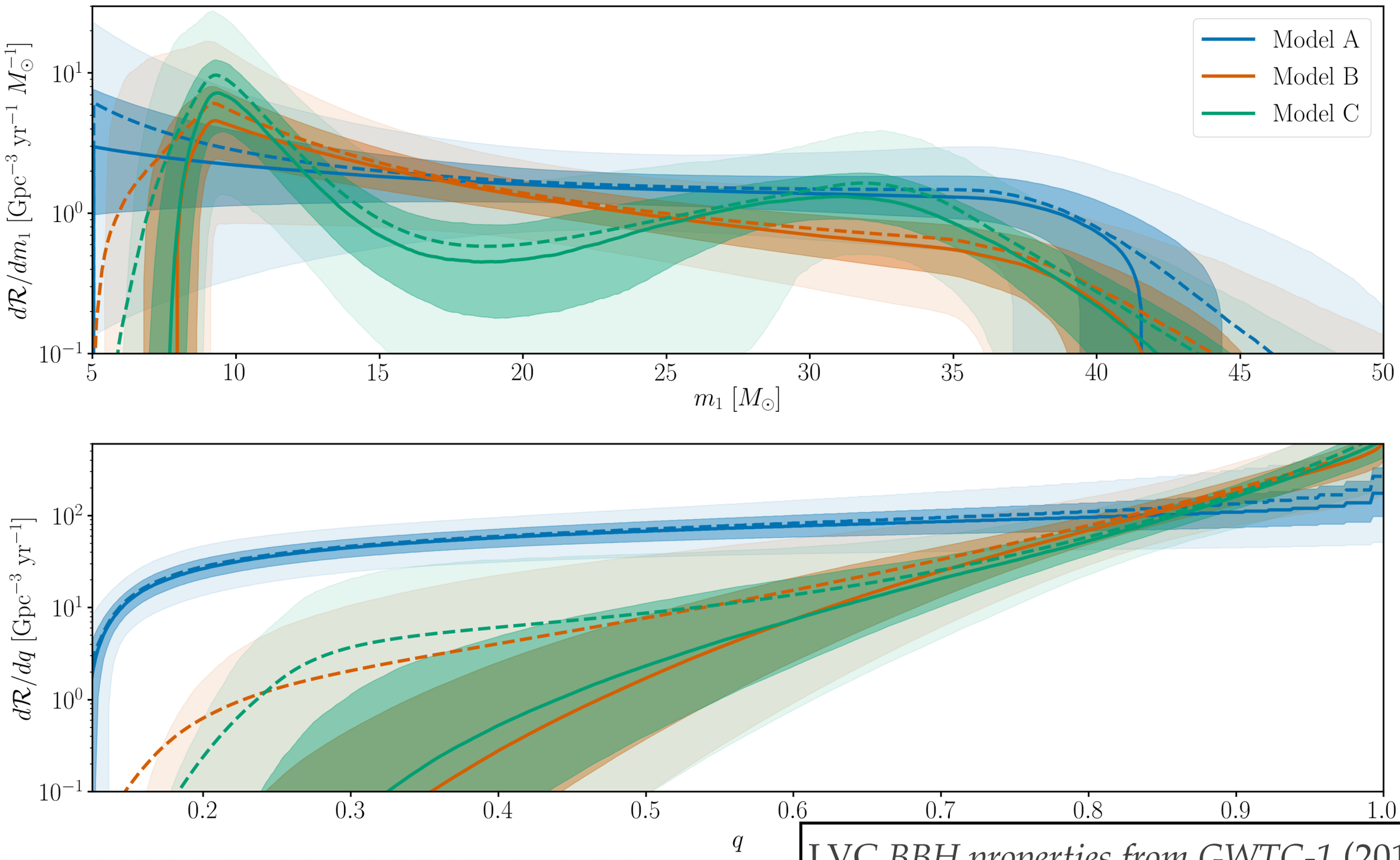

LVC *BBH properties from GWTC-1* (2019)

Population inference: spins

- Describe spin magnitude distribution using a Beta distribution (support is in the desired range [0,1]).

$$p(a_i|\alpha_a,\beta_a) = \frac{a_i^{\alpha_a-1}(1-a_i)^{\beta_a-1}}{\mathrm{B}(\alpha_a,\beta_a)}$$

- Or using a non-parametric model where the fraction of spin magnitudes in different bins are the hyperparameters, e.g., 3-bin model.

$$p(a) = \begin{cases} A_1/3 & 0 \leq a < 1/3 \\ A_2/3 & 1/3 \leq a < 2/3 \\ (1-(A_1+A_2))/3 & 2/3 \leq a \leq 1 \end{cases}$$

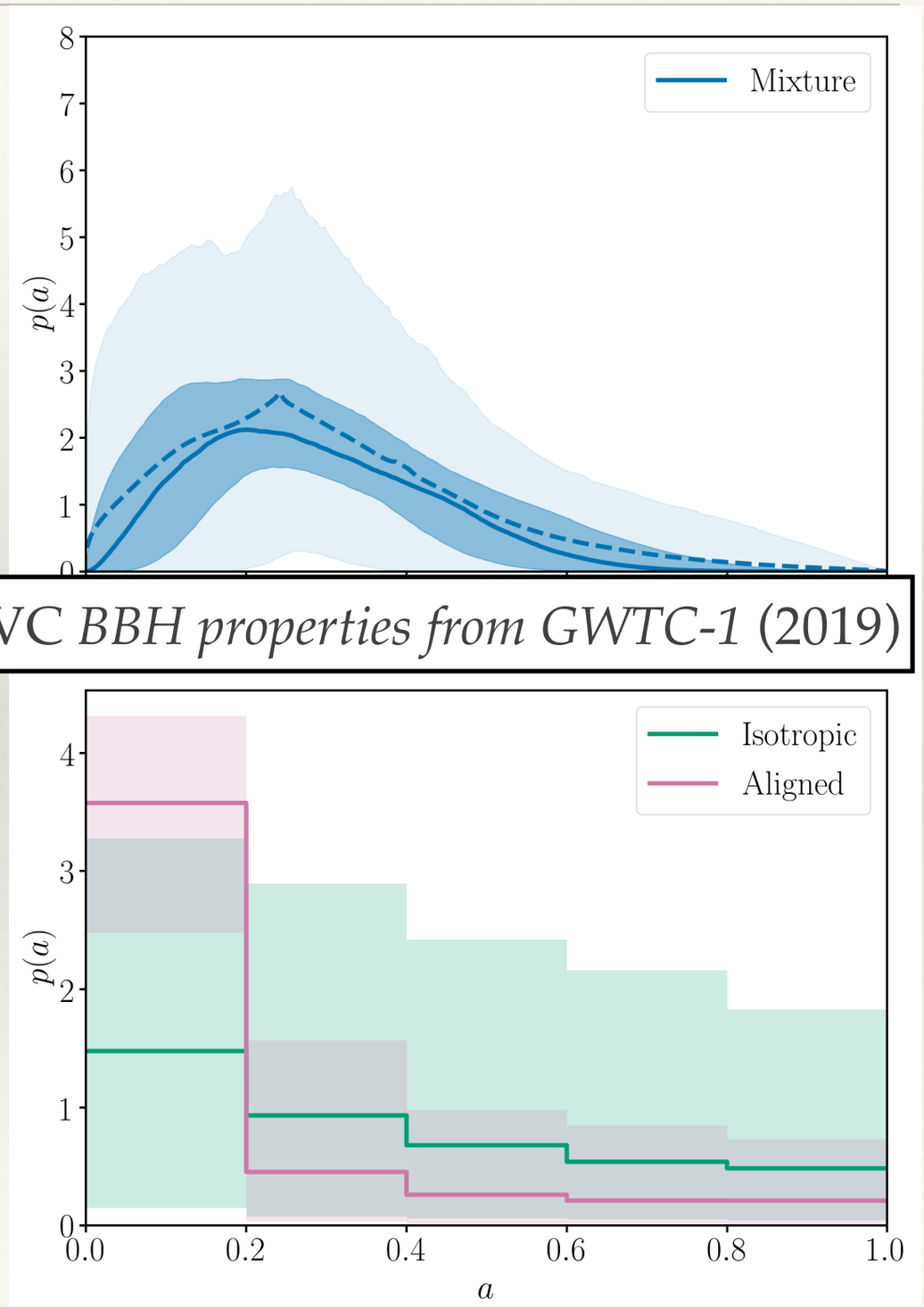

LVC *BBH properties from GWTC-1* (2019)

Population inference: spins

- Probe binary formation mechanisms by constraining spin distribution as a combination of an isotropic component, and a preferentially aligned component.

$$p(\cos t_1, \cos t_2 | \sigma_1, \sigma_2, \zeta) = \frac{(1-\zeta)}{4} + \frac{2\zeta}{\pi} \prod_{i \in \{1,2\}} \frac{\exp\left(-(1-\cos t_i)^2/(2\sigma_i^2)\right)}{\sigma_i \mathrm{erf}(\sqrt{2}/\sigma_i)}$$

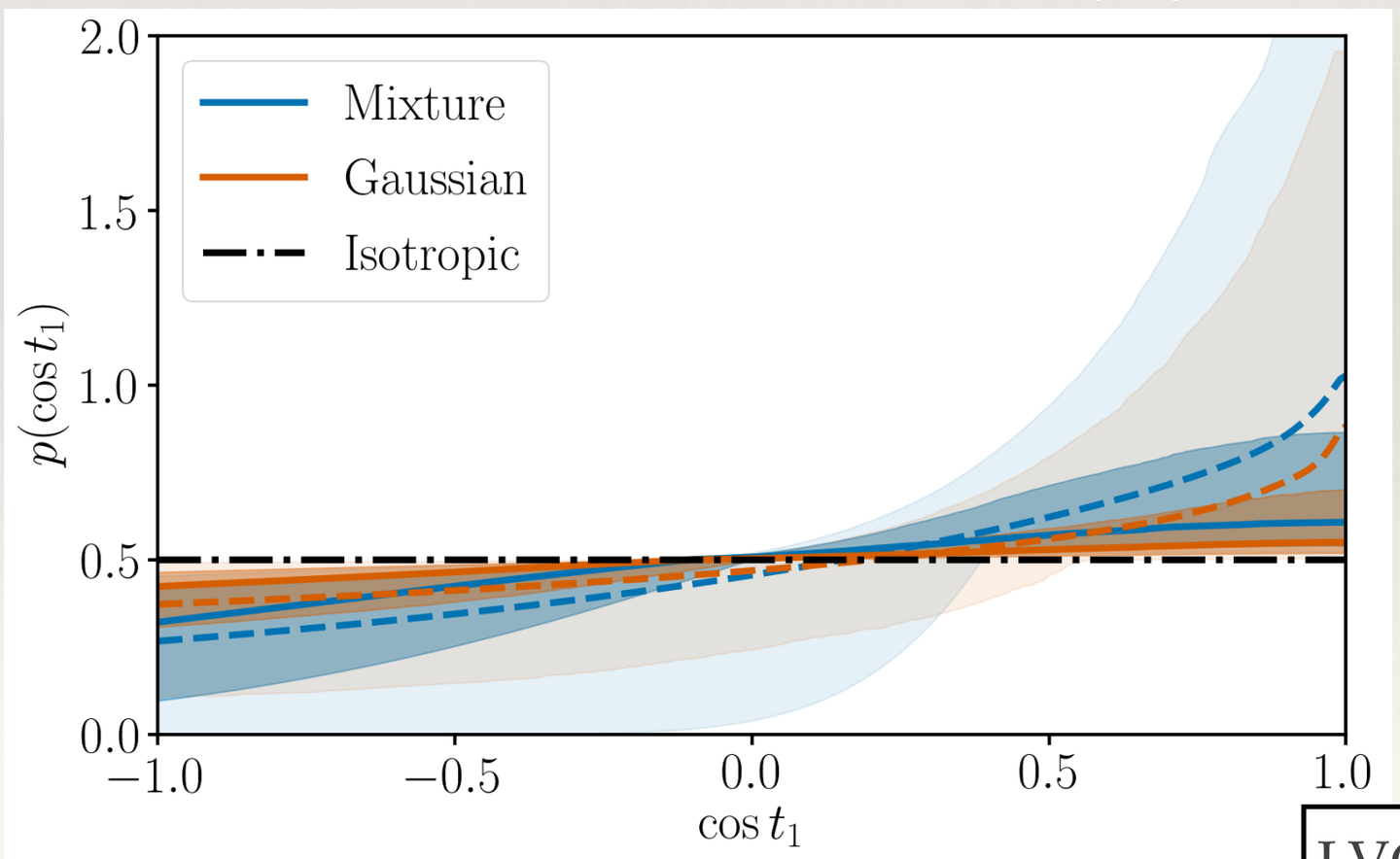

- Gaussian (G): $\zeta = 1$.
- Mixture (M): $0 \leq \zeta \leq 1$.

LVC *BBH properties from GWTC-1* (2019)

Population inference: rate evolution

- Constrain evolution of the rate of BBH mergers by including redshift dependence in the rate model

$$\frac{\mathrm{d}R}{\mathrm{d}\xi}(z|\theta) = R_0 p(\xi|\theta)(1+z)^{\lambda}$$

- Generate combined constraints on the rate evolution exponent and the parameters of the simple power-law mass function (model A).

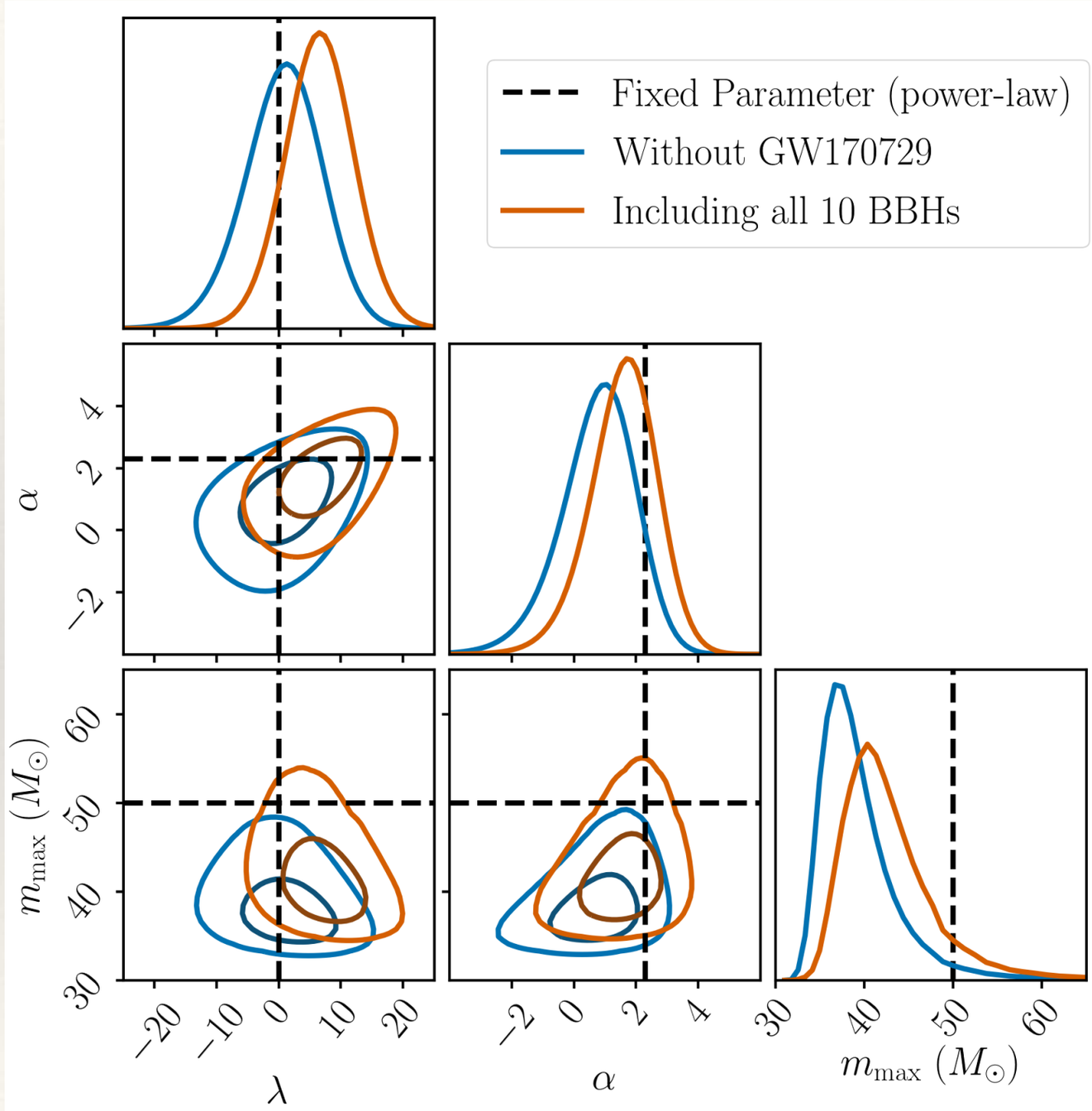

LVC *BBH properties from GWTC-1* (2019)

Model selection

Model selection

- Bayesian inference is also used for model selection based on the **evidence ratio** or **Bayes factor**.

- Example applications to LIGO include
  - test for presence/absence of gravitational radiation after the merger of a binary neutron star;
  - test of GW polarisation - tensor versus scale or vector polarisations.

LVC, *Phys. Rev.* X **9** 011001 (2019)

We determine the relative evidence for two models: that the on-source data are described by Gaussian noise only, or by Gaussian noise plus a GW signal as described in Refs. [151,152]. We find that the Gaussian noise model is strongly preferred, with a Bayes factor (evidence ratio) of 256.79 over the signal model. This result is consistent with both prompt collapse to a BH and with a postmerger signal that is too weak to be measurable with our current sensitivity. We further characterize the absence of a

LVC, *Phys. Rev.* D **100** 104036 (2019)

The Bayes factors (marginalized likelihood ratios) obtained in this case are 12 ± 3 for tensor vs vector and 407 ± 100 for tensor vs scalar, where the error corresponds to the uncertainty due to discrete sampling in the evidence computations. These values are comparable to those from GW170814, for which the latest recalibrated and cleaned data (cf. Sec. II) yield Bayes factors of 30 ± 4 and 220 ± 27 for tensor vs vector and scalar respectively.[22] Values from these binary black holes are many orders of magnitude weaker than those obtained from GW170817, where we benefited from the precise sky-localization provided by an electromagnetic counterpart [8].

Model selection

- **Tests of no-hair property**: use evidence to quantify evidence for ringdown modes different to those predicted by general relativity.

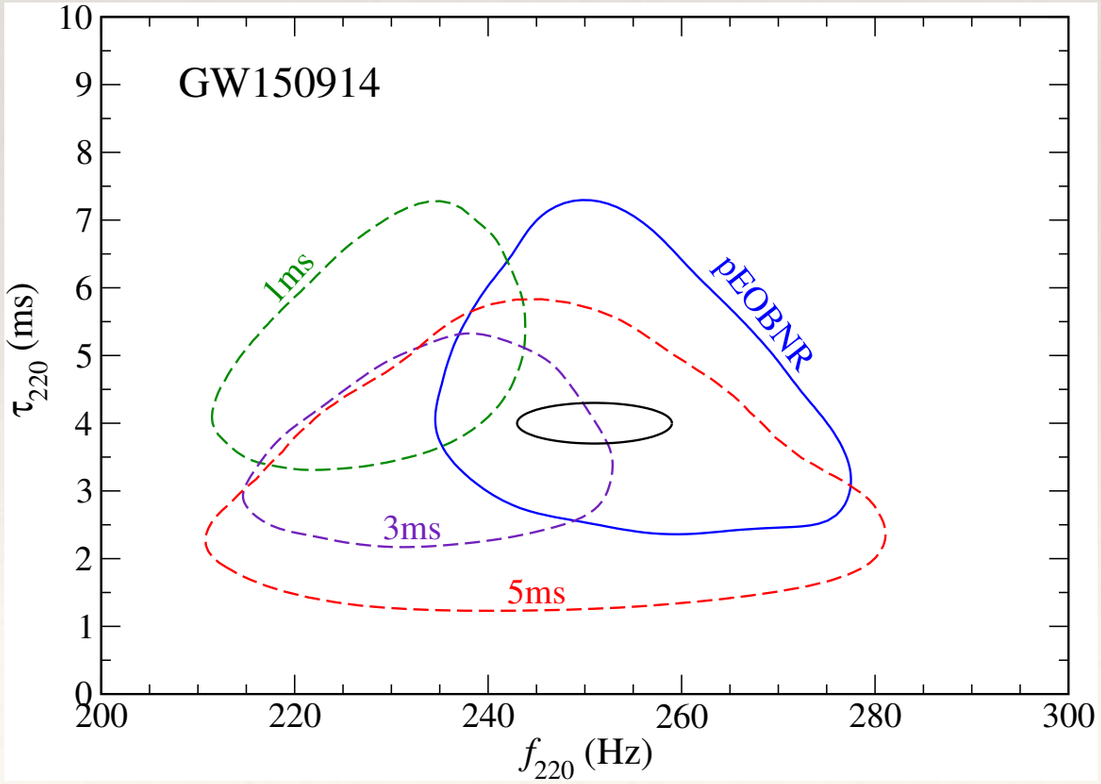

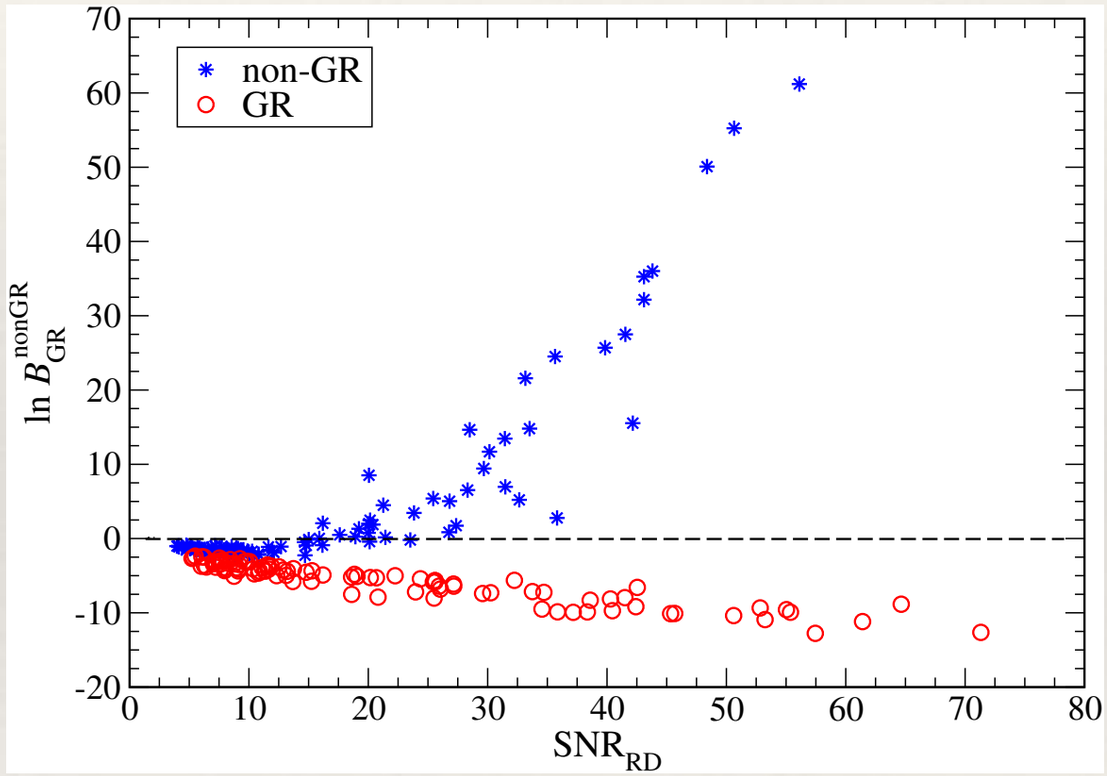

Brito, Buonanno, Raymond (2019)

Model selection

- Another example: *Probing dynamical gravity with the polarisation of continuous gravitational waves, Isi et al. (2017) Phys. Rev. D* ***96*** *042001.* (not yet a LIGO search).

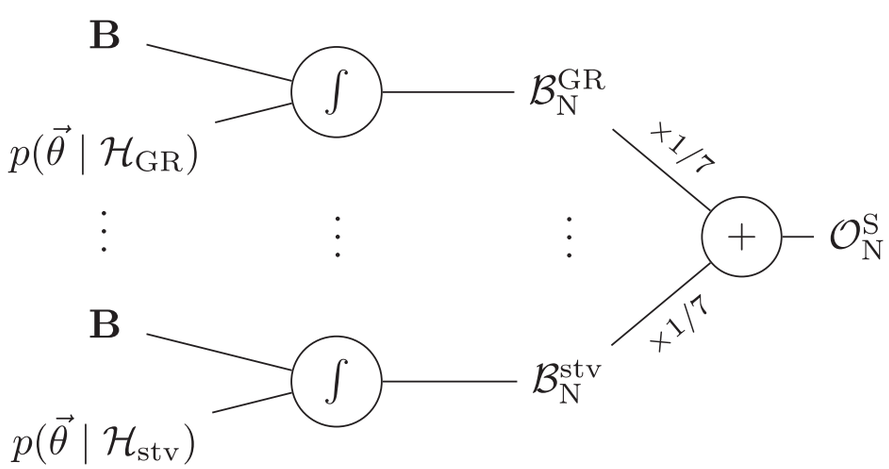

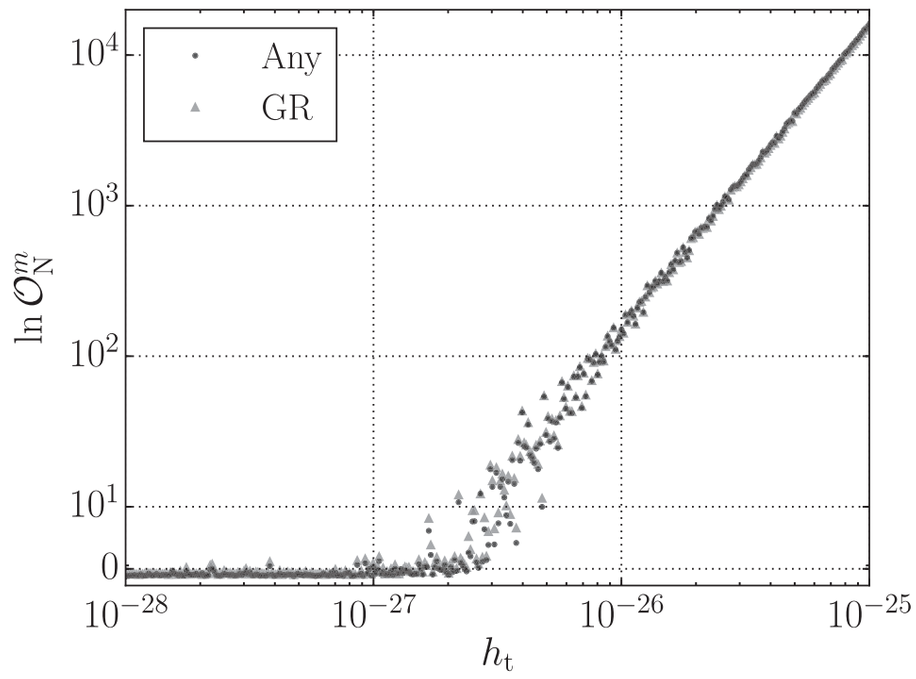

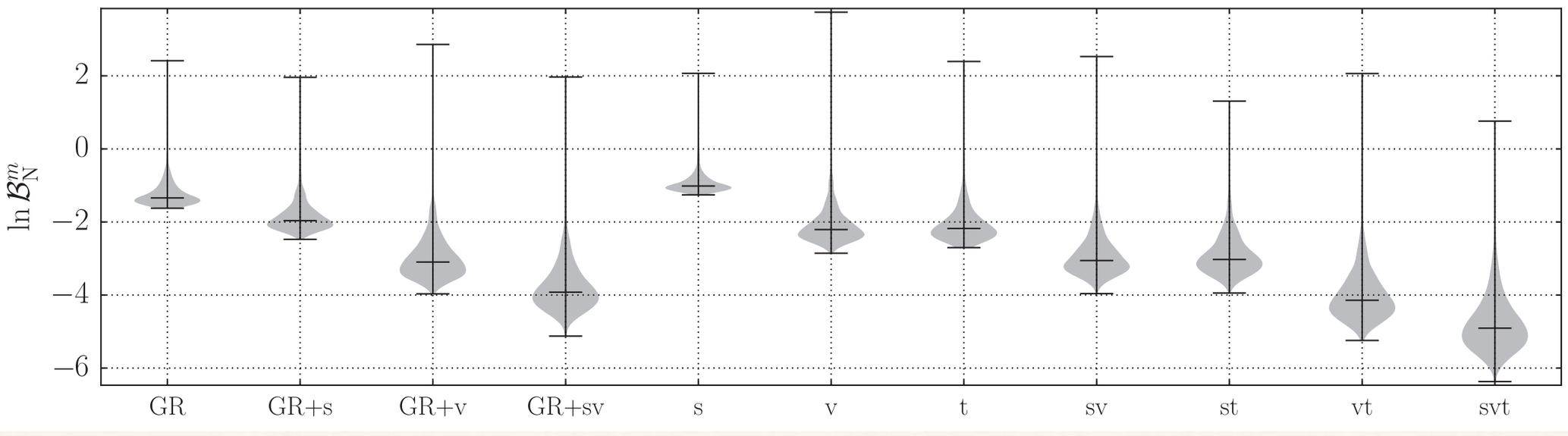

Source reconstruction

BayesWave

- The *BayesWave* pipeline uses a Bayesian non-parametric approach to reconstruct noise and signal components from the data.
- The smooth noise PSD component is modelled using a cubic spline.
- Lines in the instrumental noise are modelled using Lorentzian functions.

$$p(x; b, m) = \frac{1}{\pi} \frac{b}{(x-m)^2 + b^2}$$

- The remaining components of the data are modelled using *wavelets,* which resolve time series at particular times and frequencies. *BayesWave* uses the Morley-Gabor basis.
- There is a coherent wavelet component for sources and incoherent components to represent glitches.

BayesWave

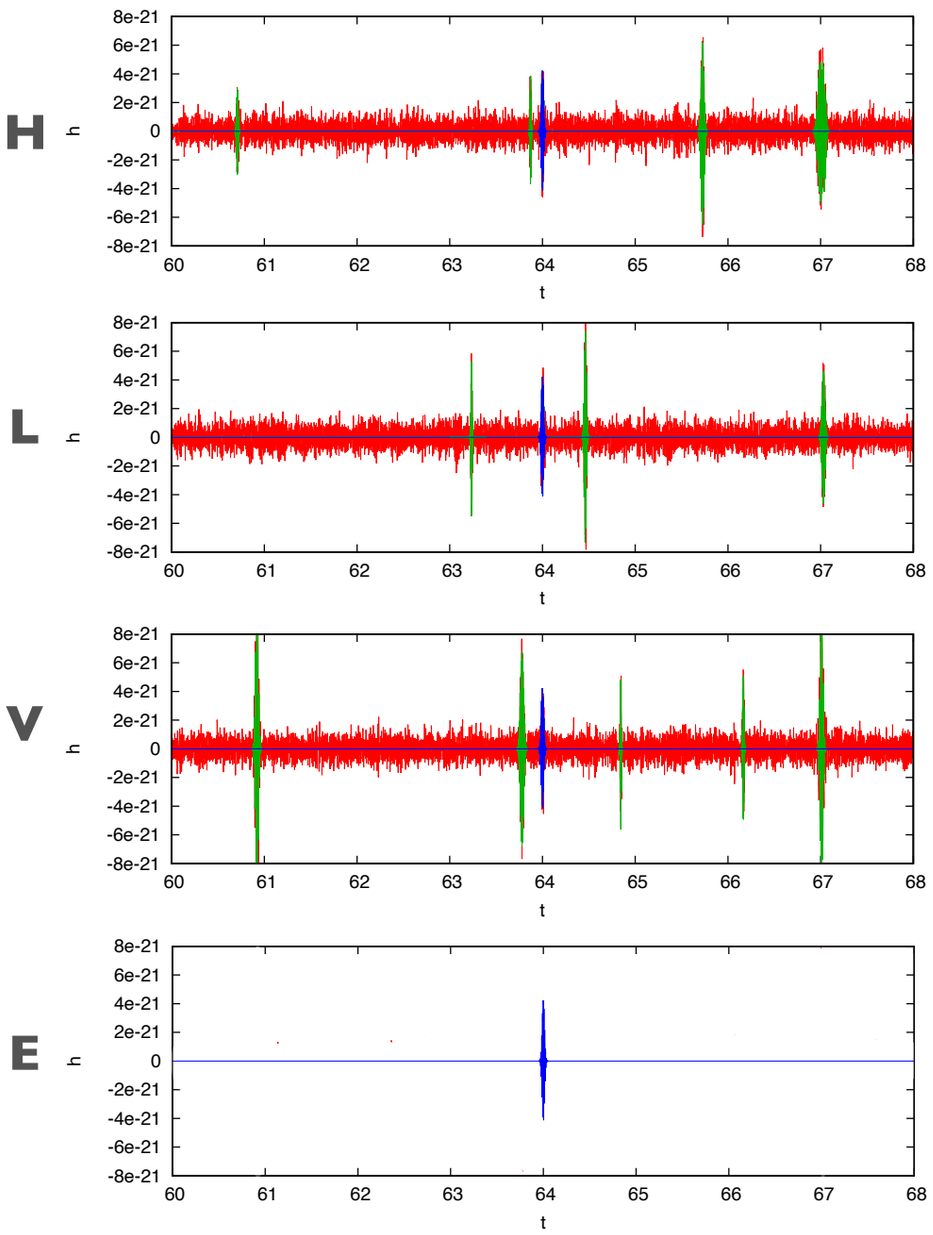

Independent

Coherent

$$d^H = n^H + \sum_i^{N_G^H} \psi(\vec{\gamma}_i^H) + h^H(N_{\rm GW}^{\oplus}, \vec{\gamma}^{\oplus}, \vec{\lambda}\,)$$

$$d^L = n^L + \sum_i^{N_G^L} \psi(\vec{\gamma}_i^L) + h^L(N_{\rm GW}^{\oplus}, \vec{\gamma}^{\oplus}, \vec{\lambda}\,)$$

$$d^V = n^V + \sum_i^{N_G^V} \psi(\vec{\gamma}_i^V) + h^V(N_{\rm GW}^{\oplus}, \vec{\gamma}^{\oplus}, \vec{\lambda}\,)$$

$$h^{\rm IFO} = \mathcal{R}^{IFO}(\vec{\lambda}) * \sum_i^{N_{\rm GW}^{\oplus}} \psi(\vec{\gamma}_i^{\oplus})$$

Extrinsic

Intrinsic

$\{\vec{\Omega}, \delta\phi_{\oplus}, \delta t_{\oplus}, \delta\mathcal{A}, \psi, e\}$

sky location, orientation, etc.

$\{t_0, f_0, \mathcal{A}, \text{etc.}\}$

morphological params.

BayesWave

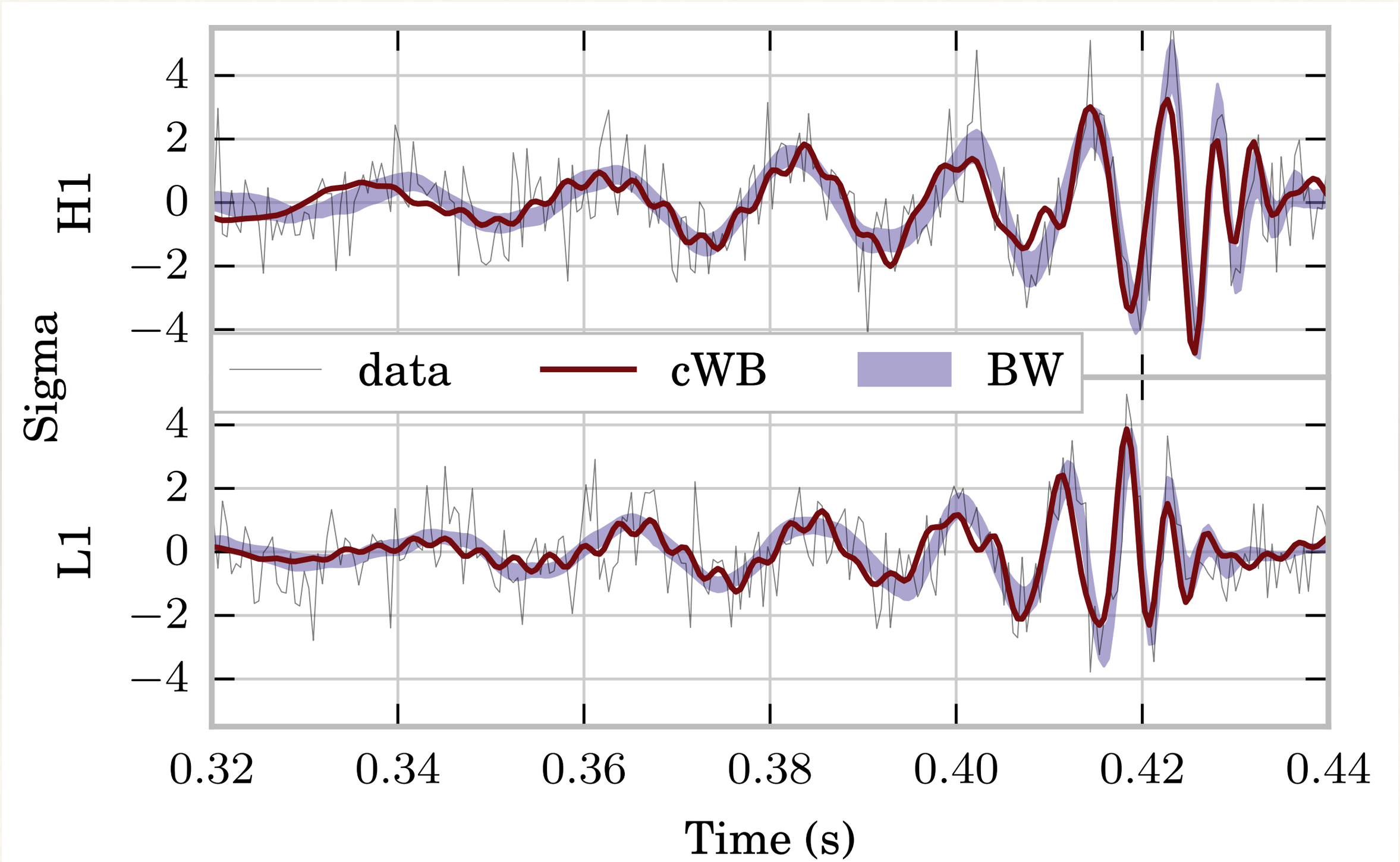

Rapid localisation

Bayestar

- Bayesian techniques are also used to obtain rapid sky localisation of GW transients to send triggers to astronomers for EM follow-up.

- **Bayestar** employs the **autocorrelation likelihood** (likelihood evaluated at MLE parameter values)

$$\exp\left[-\frac{1}{2}\sum_i {\rho_i}^2 + \sum_i \rho_i \Re\left\{e^{-i\gamma_i} z_i^*(\tau_i)\right\}\right]$$

- Rapid marginalisation over parameters other than sky location achieved via integral approximation and look-up tables.

- Result is a sky map probability density.

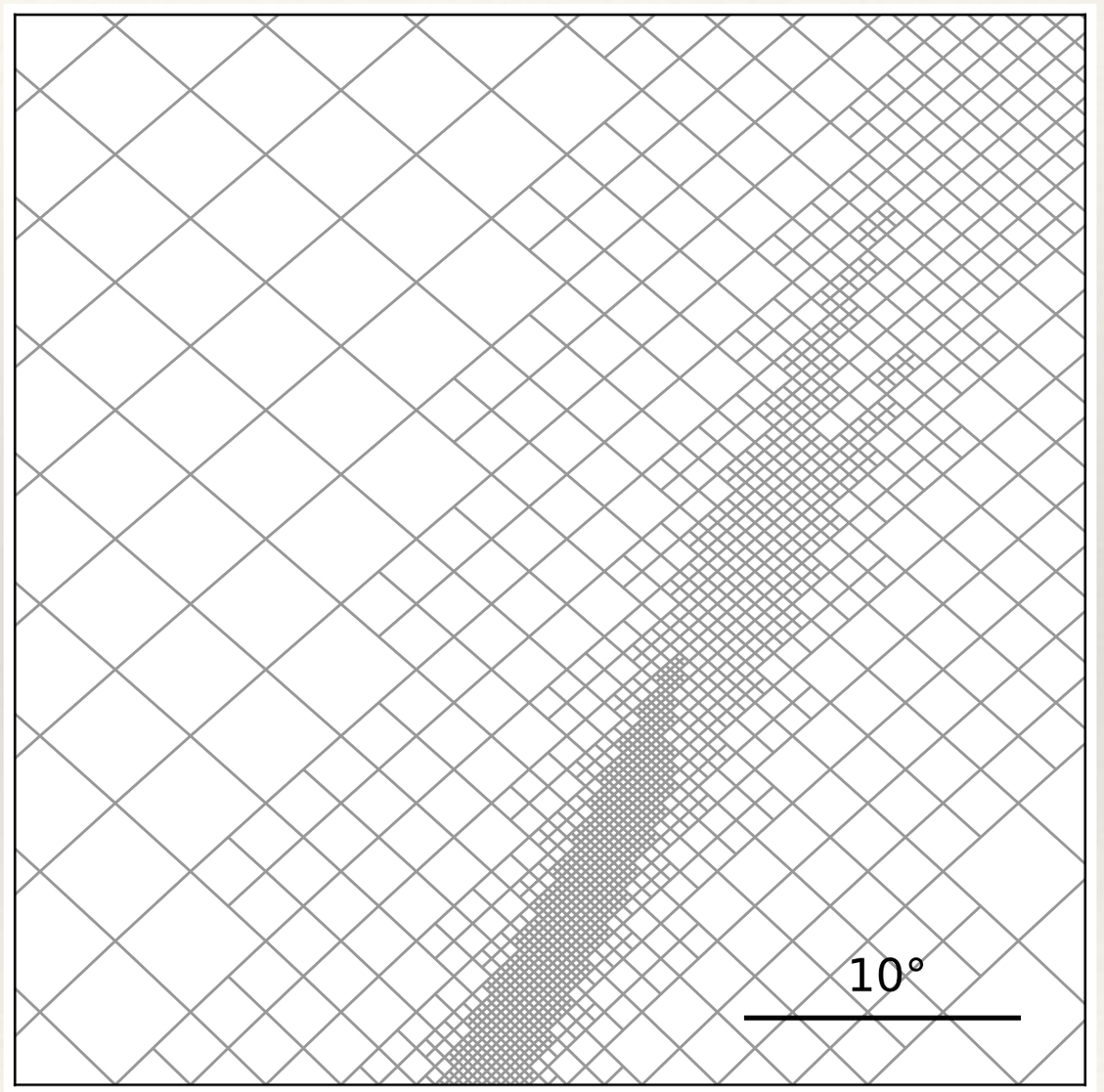

Singer & Price (2015)

Bayestar

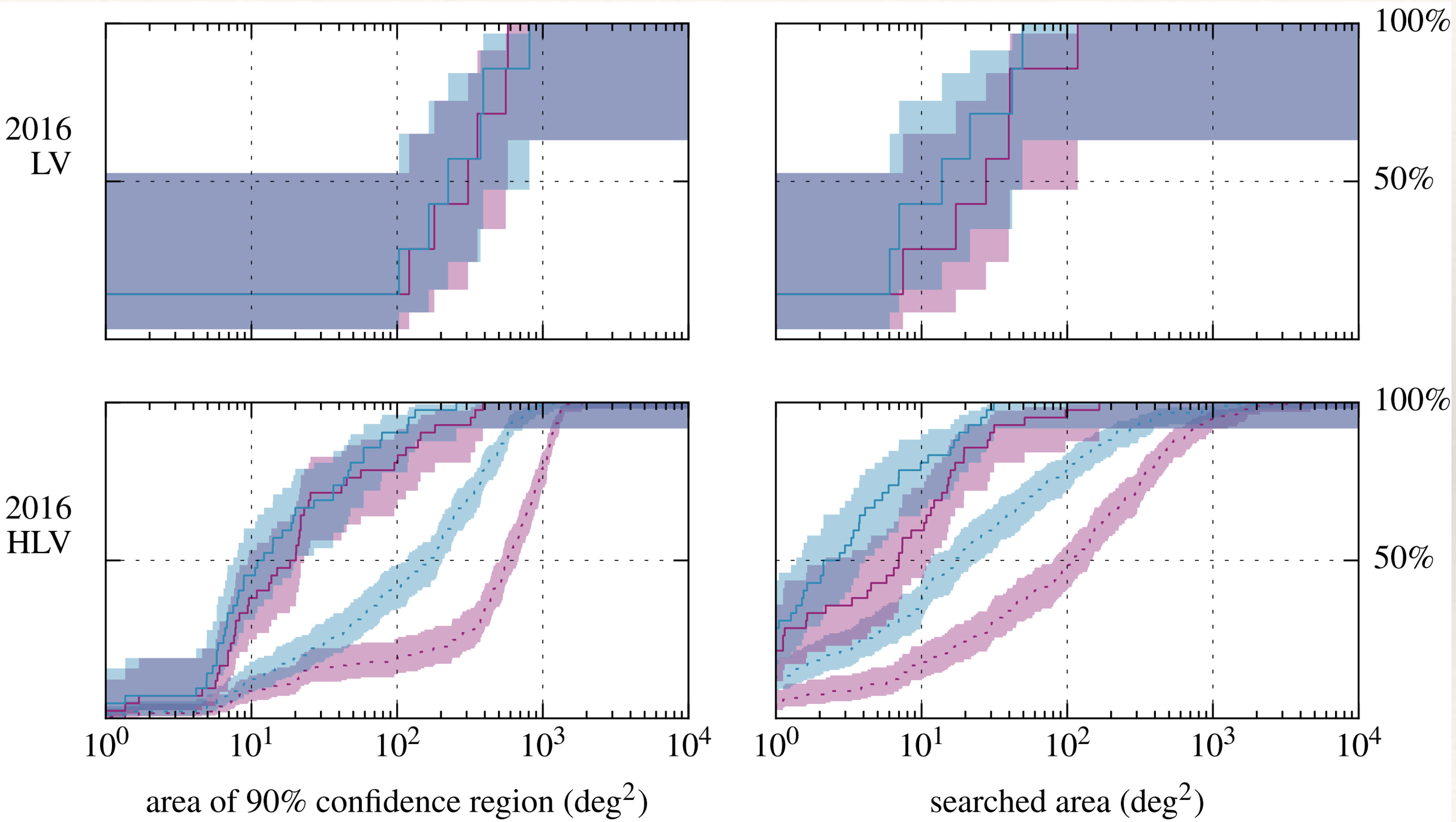

Singer & Price (2015)

LALInference Burst

- *LALInference Burst* is another tool for rapid source localisation. The signal is modelled as a sine-Gaussian, coherent between detectors.

$$h_\times(t) = \sin(\alpha)\frac{h_{\rm rss}}{\sqrt{Q(1-\cos(2\phi_o)\,e^{-Q^2})/4f_o\sqrt{\pi}}} \times \sin(2\pi f_o(t-t_o)+\phi_o)\,e^{-(t-t_o)^2/\tau^2}$$

$$h_+(t) = \cos(\alpha)\frac{h_{\rm rss}}{\sqrt{Q(1+\cos(2\phi_o)\,e^{-Q^2})/4f_o\sqrt{\pi}}} \times \cos(2\pi f_o(t-t_o)+\phi_o)\,e^{-(t-t_o)^2/\tau^2}.$$

- Figure of merit (left) is sky area searched before true sky location identified.

- Bayestar and LIB are not true Bayesian algorithms since model of data generation process is approximated.

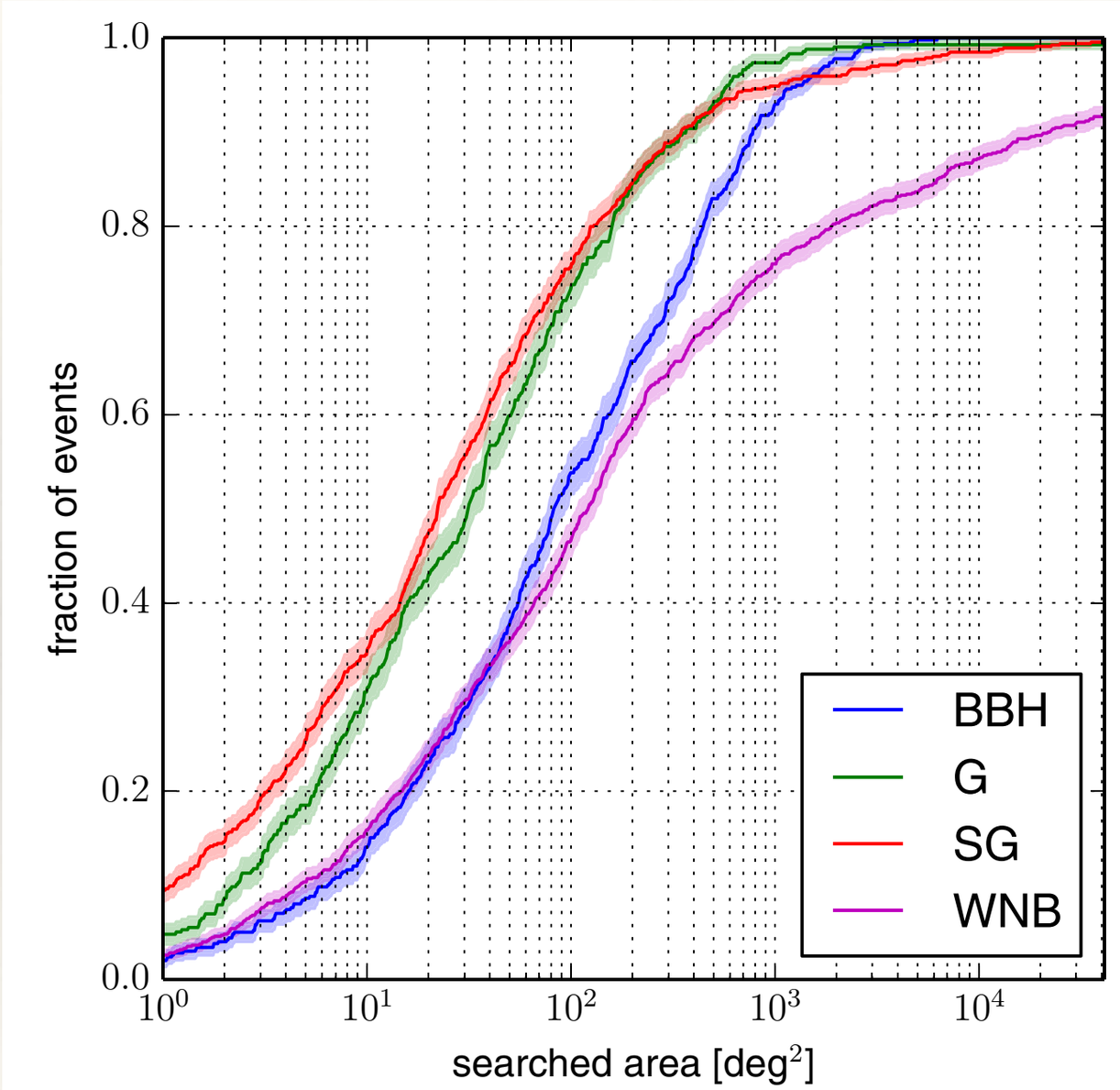

Essick et al. (2015)

oLIB

- There is also an online version of LIB, that mixes frequentist and Bayesian techniques.
- LIB is used to compute **Bayes factors** for the signal versus noise hypothesis (BSN) and for **coherent** versus **incoherent** triggers across detectors (BCI).
- oLIB, along with CWB, were the first algorithms to detect GW150914, as they were the online online algorithms running at the start of O1.

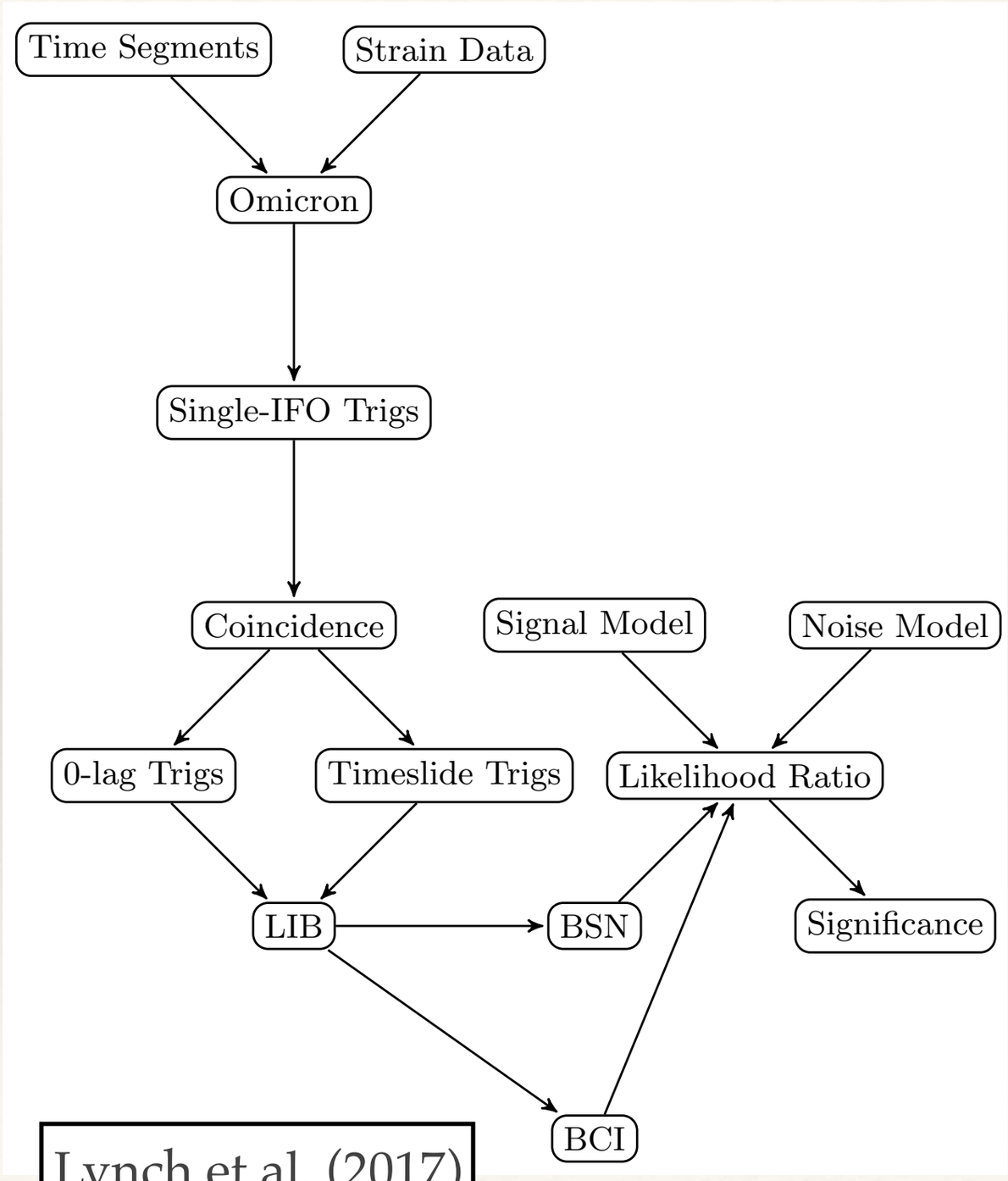

Lynch et al. (2017)

Parameter estimation: LISA

Parameter estimation for LISA

- Parameter estimation (and some searches) in the Mock LISA Data Challenges used Bayesian methods, such as MCMC.

source ($\mathrm{SNR}_{\mathrm{true}}$)	group	$\Delta M_c/M_c$ $\times 10^{-5}$	$\Delta\eta/\eta$ $\times 10^{-4}$	Δt_c (sec)	Δsky (deg)	Δa_1 $\times 10^{-3}$	Δa_2 $\times 10^{-3}$	$\Delta D/D$ $\times 10^{-2}$	SNR	FF_A	FF_E
MBH-1	AEI	2.4	6.1	62.9	11.6	7.6	47.4	8.0	1657.71	0.9936	0.9914
(1670.58)	CambAEI	3.4	40.7	24.8	2.0	8.5	79.6	0.7	1657.19	0.9925	0.9917
	MTAPC	24.8	41.2	619.2	171.0	13.3	28.7	4.0	1669.97	0.9996	0.9997
	JPL	40.5	186.6	23.0	26.9	39.4	66.1	6.9	1664.87	0.9972	0.9981
	GSFC	1904.0	593.2	183.9	82.5	5.7	124.3	94.9	267.04	0.1827	0.1426
MBH-3	AEI	9.0	5.2	100.8	175.9	6.2	18.6	2.7	846.96	0.9995	0.9989
(847.61)	CambAEI	13.5	57.4	138.9	179.0	21.3	7.2	1.5	847.04	0.9993	0.9993
	MTAPC	333.0	234.1	615.7	80.2	71.6	177.2	16.1	842.96	0.9943	0.9945
	JPL	153.0	51.4	356.8	11.2	187.7	414.9	2.7	835.73	0.9826	0.9898
	GSFC	8168.4	2489.9	3276.9	77.9	316.3	69.9	95.6	218.05	0.2815	0.2314
MBH-4	AEI	4.5	75.2	31.4	0.1	47.1	173.6	9.1	160.05	0.9989	0.9994
(160.05)	CambAEI	3.2	171.9	30.7	0.2	52.9	346.1	21.6	160.02	0.9991	0.9992
	MTAPC	48.6	2861.0	5.8	7.3	33.1	321.1	33.0	149.98	0.8766	0.9352
	JPL	302.6	262.0	289.3	4.0	47.6	184.5	28.3	158.34	0.8895	0.9925
	GSFC	831.3	1589.2	1597.6	94.4	59.8	566.7	95.4	−45.53	−0.1725	−0.2937
MBH-2	AEI	1114.1	952.2	38160.8	171.1	331.7	409.0	15.3	20.54	0.9399	0.9469
(18.95)	CambAEI	88.7	386.6	6139.7	172.4	210.8	130.7	24.4	20.36	0.9592	0.9697
	MTAPC	128.6	45.8	16612.0	8.9	321.4	242.4	13.1	20.27	0.9228	0.9260
	JPL	287.0	597.7	11015.7	11.8	375.3	146.3	9.9	18.69	0.9661	0.9709
MBH-6	AEI	1042.3	1235.6	82343.2	2.1	258.2	191.6	26.0	13.69	0.9288	0.9293
(12.82)	CambAEI	5253.2	1598.8	953108.0	158.3	350.8	215.4	29.4	10.17	0.4018	0.4399
	MTAPC	56608.7	296.7	180458.8	119.7	369.2	297.6	25.1	11.34	-0.0004	0.0016

Parameter estimation for LISA

- Multi stage approach used for EMRIs.
- Final PE phase employed MCMC to obtain parameter posteriors.

type[1]	ν (mHz)	$\mu/M_\odot$	$M/M_\odot$	e_0	θ_S	φ_S	λ	a/M^2	SNR
True	0.1920421	10.296	9517952	0.21438	1.018	4.910	0.4394	0.69816	120.5
Found	0.1920437	10.288	9520796	0.21411	1.027	4.932	0.4384	0.69823	118.1
True	0.34227777	9.771	5215577	0.20791	1.211	4.6826	1.4358	0.63796	132.9
Found	0.34227742	9.769	5214091	0.20818	1.172	4.6822	1.4364	0.63804	132.8
True	0.3425731	9.697	5219668	0.19927	0.589	0.710	0.9282	0.53326	79.5
Found	0.3425712	9.694	5216925	0.19979	0.573	0.713	0.9298	0.53337	79.7
True	0.8514396	10.105	955795	0.45058	2.551	0.979	1.6707	0.62514	101.6
Found	0.8514390	10.106	955544	0.45053	2.565	1.012	1.6719	0.62534	96.0
True	0.8321840	9.790	1033413	0.42691	2.680	1.088	2.3196	0.65829	55.3
Found	0.8321846	9.787	1034208	0.42701	2.687	1.053	2.3153	0.65770	55.6
Blind									
True	0.1674472	10.131	10397935	0.25240	2.985	4.894	1.2056	0.65101	52.0
Found	0.1674462	10.111	10375301	0.25419	3.023	4.857	1.2097	0.65148	51.7
True	0.9997627	9.7478	975650	0.360970	1.453	4.95326	0.5110	0.65005	122.9
Found	0.9997626	9.7479	975610	0.360966	1.422	4.95339	0.5113	0.65007	116.0

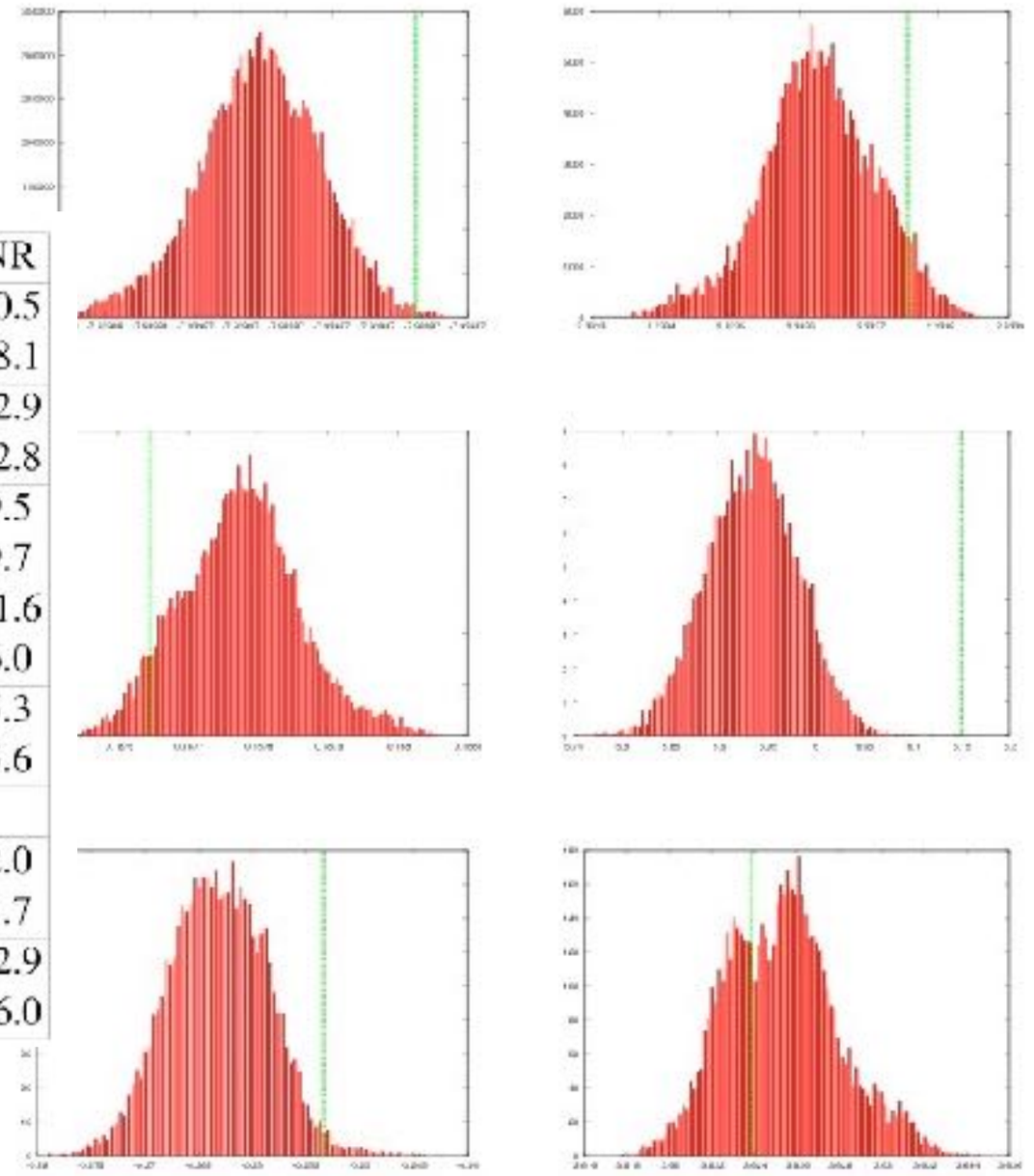

Babak, JG & Porter (2009)

Nested Sampling for GWs: MultiNest

- MultiNest has been widely used in astrophysics and other fields.
- There have been a number of applications to gravitational wave detection. For example, **cosmic string** detection in the Mock LISA Data Challenges.
- Identified correct number of signals (3), and recovered waveforms with better than 99% overlap in all cases.

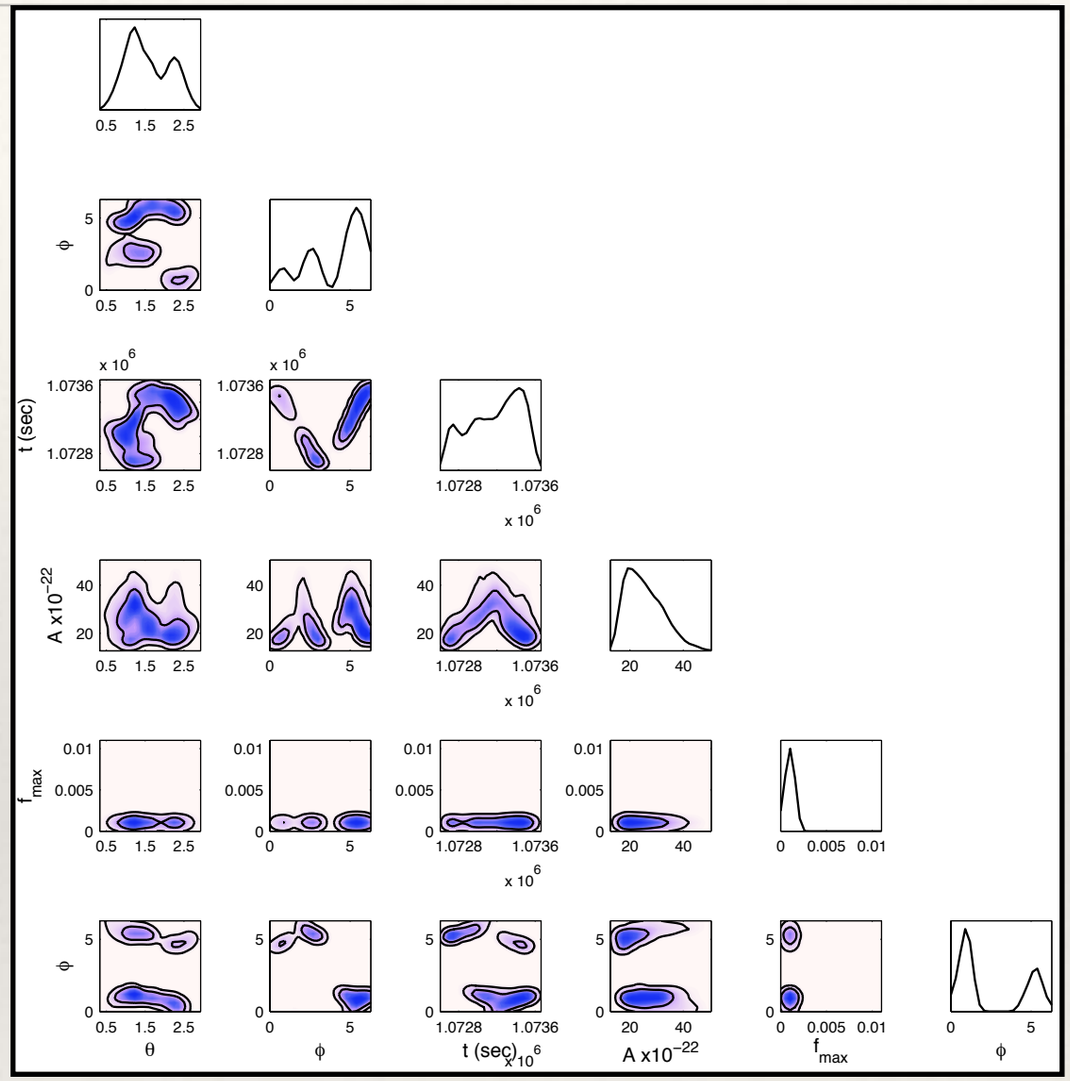

Source	t_c(s)	Channel	True SNR	Recovered SNR Mode 1	Mode 2	Mode 3
1	1.6×10^6	A E	41.0 14.5	41.2 14.5	41.0 14.6	N/A
2	1.1×10^6	A E	30.7 13.9	30.7 13.9	N/A	N/A
3	6×10^5	A E	18.8 36.9	18.9 36.7	18.5 37.1	18.4 36.8

Nested Sampling for GWs: MultiNest

- MultiNest has been widely used in astrophysics and other fields.
- There have been a number of applications to gravitational wave detection. For example, **cosmic string** detection in the Mock LISA Data Challenges.
- Identified correct number of signals (3), and recovered waveforms with better than 99% overlap in all cases.
- Evidence ratio identifies burst origin as cosmic string versus generic sine-Gaussian alternative.